POLITECNICO
MILANO 1863

SCUOLA DI INGEGNERIA INDUSTRIALE
E DELL'INFORMAZIONE

Model-free Control of Actuated Tendon-Driven MitraClip™ Catheter

Tesi di Laurea Magistrale in
Biomedical Engineering - Ingegneria Biomedica

Author: **Mariagrazia Quacquarelli**

Student ID: 968372
Advisor: Prof. Elena De Momi
Co-advisors: Ph.D. Anna Bicchi, Mattia Magro
Academic Year: 2021-22

Abstract

The incidence of Structural Heart Diseases (SHDs), a defect or disorder in the heart's structures, is increasing, primarily due to ageing population. Among SHDs, Mitral Regurgitation is the leading cause of death, affecting 10% of the global population with a mortality rate increasing annually of 1.5%. Recently, Structural Intervention Cardiology has emerged as a specialized medical field, treating patients with a minimally invasive, transcatheter approach. For mitral valve repair, the commercial MitraClip™ system is considered the Gold Standard. However, its difficult manoeuvrability and the use of fluoroscopy imaging, exposes patients to more risks and operators to high mental work and damaging X-ray radiations. Therefore, ARTERY project is born with the goal of overcoming the limitations of a manual transcatheter approach, through the use of a robot-assisted platform with autonomous control. In a previous work, a robotic platform with autonomous control for this system was presented. However, it has limitations as reduced DoF, modelling approximations and suboptimal control. Therefore, the aim of the thesis is to overcome these issues by proposing a different methodology comprising two parts. The first one, is to re-design the system in Solidworks®, adding some features and DoF that were missing. The second is to implement a model-free closed-loop control with neural networks to improve the accuracy in terms of position and orientation of the catheter's tip. To test this approach, electrical motors are integrated and actuated by a micro-controller. Furthermore, electromagnetic sensors are embedded in the catheter to track real-time pose of the clip. The experiments involved a path tracking task, tested on the designed system, implementing both the previous control approach and the presented one. The results show improved outcomes in the model-free approach, reaching an accuracy of 2.37±0.13 mm for position and below 10° for all angles orientation, which was not controlled before. These results, demonstrate the feasibility of using model-free controllers in highly non-linear system as this one, reaching better accuracy compared to model-based controllers.

Keywords: Structural Intervention Cardiology, robot-assisted surgery, tendon-driven robotic actuation, continuum robot, model-free control

Sommario

L'incidenza di malattie cardiovascolari, ovvero difetti o disturbi cardiaci, è in aumento, soprattutto a causa dell'invecchiamento della popolazione. Tra questi, il regurgito mitralico è la principale causa di morte, che colpisce il 10% della popolazione con un tasso di mortalità che aumenta annualmente del 1,5%. Recentemente, la Cardiologia Interventistica Strutturale è emersa come campo medico, trattando i pazienti con approccio mininvasivo e transcatetere. Per la riparazione della valvola mitrale, il sistema MitraClip™ è considerato lo standard. Tuttavia, la sua difficile manovrabilità e l'uso della fluoroscopia espongono i pazienti a maggiori rischi e gli operatori a un alto carico mentale e radiazioni dannose. Dunque, il progetto ARTERY nasce con l'obiettivo di superare i limiti di questo approccio attraverso l'uso di una piattaforma robotica autonoma. In un precedente lavoro, è stata presentata una piattaforma robotica per questo sistema. Tuttavia, presenta limitazioni come ridotti GdL, modello approssimato e controllo subottimale. Pertanto, l'obiettivo della tesi è di superare questi limiti proponendo una diversa metodologia descritta in due parti. La prima consiste nel riprogettare il sistema in Solidworks®, aggiungendo caratteristiche e GdL che mancavano. La seconda consiste nell'implementare un controllo ad anello chiuso con reti neurali per migliorare la precisione in termini di posizione e orientamento della clip. Nella fase di test, sono stati usati motori elettrici azionati da microcontrollore. Inoltre, sono stati integrati sensori elettromagnetici per tracciare in tempo reale la posizione della clip. In seguito, sono stati eseguiti esperimenti di path-tracking sul sistema progettato, implementando sia il controllo precedente che quello presentato. I risultati mostrano un miglioramento nell'approccio con reti neurali, raggiungendo un'accuratezza di 2.37 ± 0.13 mm in posizione e inferiore a 10° in orientamento, non precedentemente controllato. Questi risultati dimostrano la fattibilità dell'uso di reti neurali nel controllo di sistemi non lineari come questo, raggiungendo una migliore accuratezza rispetto ai controllori basati su modello.

Parole chiave: Cardiologia Interventistica Strutturale, chirurgia robotica, robot continui, cotrollo model-free, controllo a reti neurali, controllo ad anello chiuso

Contents

1 | Introduction

1.1. Clinical Context: Cardiovascular Diseases

With the increasing ageing of the population, Cardiovascular Diseases (CVDs) are the leading causes of global mortality (Figure 1.1) and major contributor to disability. CVDs belong to a class of heart diseases that involve heart and blood vessels functionality: a lack in the integrity of the anatomical components of these structures causes critical pathological effects that needs immediate intervention.

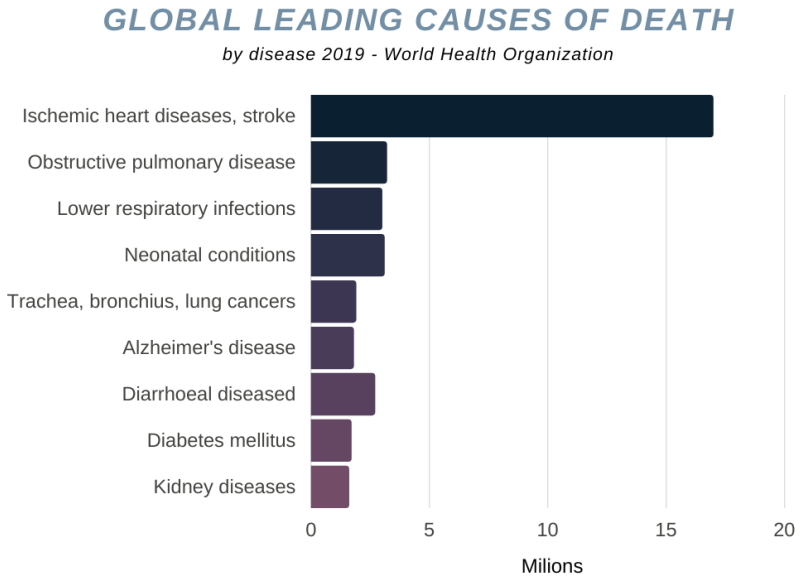

Figure 1.1: *Global top death causes in 2019, from World Health Organization.*

1.1.1. Cardiovascular Diseases: Statistics

The cases of total CVDs nearly doubled from 271 million in 1990 to 523 million in 2019. Accordingly, the number of CVD deaths steadily increased from 12.1 million reaching 18.6 million in 2019 [23] and, according to the World Health Organization (WHO), 30% of which are premature (under the age of 70). Consequently, the global trends for disability-

adjusted life also increased, as well as the years lived with disability doubled over the 1990-2019 period, which lead to higher healthcare costs. In [60], the annual economic impact of CVDs is estimated to cover 40.2% of total government healthcare expenditures which correspond to be 200 billion euros in Europe and 555 USD billions in the United States [23].

1.1.2. Cardiovascular Diseases: Structural Heart Diseases

Among all CVDs, the most occurrent ones are Structural Heart Diseases (SHDs). They all involve a defect or disorder in the structures of the heart e.g. abnormality in the structure or function of the valves, walls, chambers or muscles in the heart . The main types of SHDs are:

- Heart valve disease, a problem with any of the four valves that open and close to control blood flow;
- Cardiomyopathy, a condition that affects the heart muscles, causes the heart chamber walls to swell, thicken, or stiffen;
- Congenital heart disease, structural heart condition present at birth.

SHDs are usually the result of a congenital defect, however there is an higher prevalence of SHDs linked to functional decline, that mostly affects the elderly.

Mitral Regurgitation (MR) is the most common valvular abnormality worldwide, affecting at least 10% of the general population and approximately 15% of patients over the age of 50, showing a prevalence that increases with age [9]. From 2012, MR mortality rate has increased by about 1.5% annually and is expected to grow further [43].

1.2. Mitral Valve Regurgitation

The mitral valve is a complex anatomical and functional unit consisting of different components as the annulus, the leaflets, the tendinous cords, and the papillary muscle as illustrated in Figure 1.2.

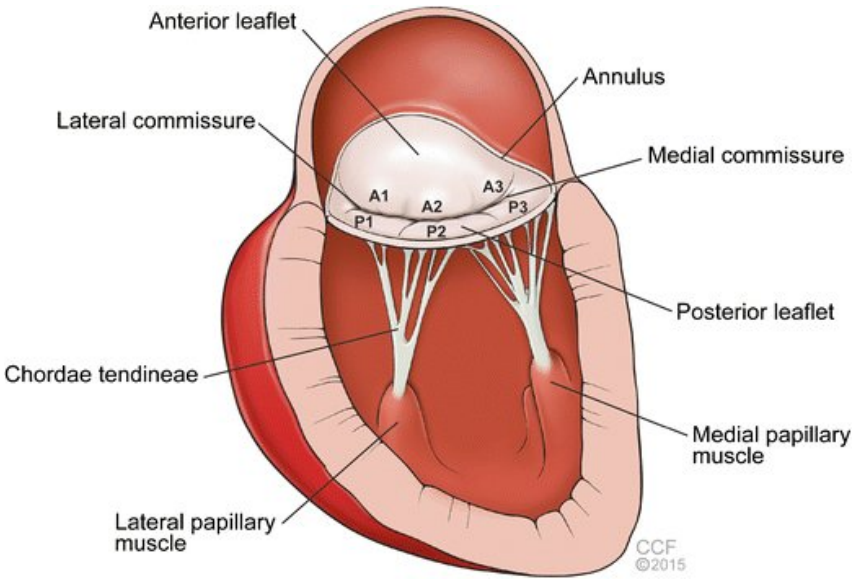

Figure 1.2: *Mitral valve anatomy. Its functional unit comprises the annulus, the leaflets, the tendinous cords, and the papillary muscle that prevents blood back-flow from left ventricle to left atrium.*

The mitral valve prevents blood back-flow to the left atrium during ventricular systole. The mechanical and metabolic balance of the valve is guaranteed by the presence of interstitial cells, which are very sensitive to mechanical information and help in valve motion. The valve surface is rich in endothelial cells that communicate with interstitial cells to maintain the strength and shape of the valve. The mitral valve requires all its components, together with the adjacent atrial and ventricular musculature, in order to work properly.

The mitral annulus is a fibrous ring located around the mitral opening, it works as a sphincter: it contracts during systole, closing the leaflets, and relaxes during diastole allowing correct blood flow.

The mitral leaflets are two, the anterior leaflet, and the posterior leaflet which comprises two-thirds of the annular circumference. The posterior leaflet is divided into three segments: P1 (lateral scallop), P2 (middle scallop), and P3 (medial scallop). The anterior leaflet has three corresponding segments: A1 (lateral portion), A2 (middle portion), and A3 (medial portion) (Figure 1.2).

The chordae tendinae are part of the sub-valvular apparatus. They and are composed of fibrous strings that originate from the papillary muscles and inserts into the anterior and posterior leaflet. Two kinds of chordae tendinae are distinguished based on their insertion into the leaflets. The primary chordae are thinner and are attached to the leaflets at

the free edge, preventing leaflet edge to prolapse. The secondary chordae are thicker and more extensible to help reduce tension at the leaflets.

The papillary muscles system coordinates with the mitral annulus, so for every contraction during systole, this system prevents leaflet prolapse. As part of the mitral apparatus, the papillary muscles work in a way to maintain proper blood flow.

If a fusion of the papillary muscles exists, it will result in stenosis of the mitral valve, and if there is a rupture of the papillary muscles or chordae tendinae, a complication of myocardial infarction will result in mitral regurgitation. In the same way, annulus dilatation can cause inadequate leaflet closure and, when severe dilation occurs, the leaflets are unable to approximate each other, and mitral regurgitation is the result.

Therefore, mitral regurgitation is associated with an abnormal backflow of blood from the left ventricle into the left atrium through the mitral valve (Figure 1.3).

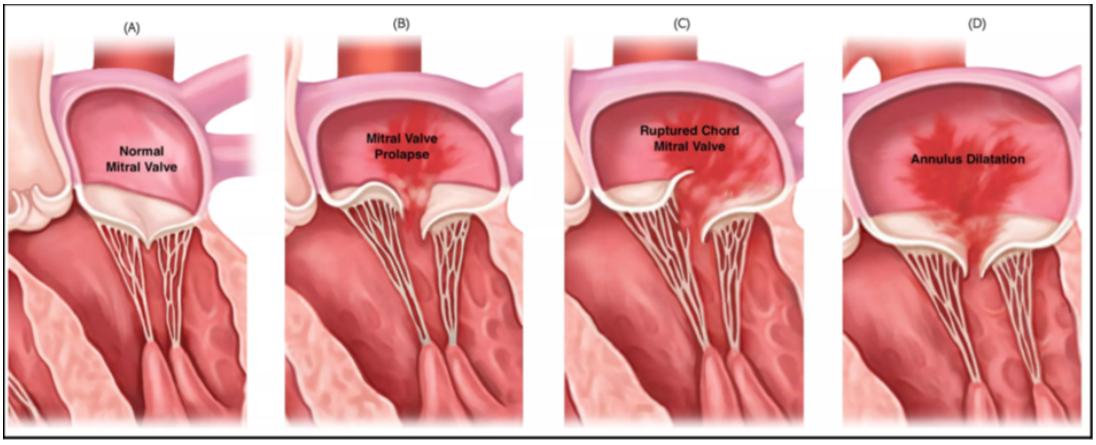

Figure 1.3: *Mitral valve regurgitation causes: (A) Normal conditions with no regurgitation; (B) Regurgitation due to valve prolapse; (C) Regurgitation due to chord rupture; (D) Regurgitation due to annulus dilatation.*

MR can be further subdivided into:

Primary or degenerative MR when prolapse or stenosis of the mitral valve occurs. Mitral Valve Prolapse (MVP) is defined as the displacement of one or more leaflets by more than 2 mm into the left atrium during ventricular systole. MVP is a common condition and also an important risk factor for developing mitral regurgitation, congestive heart failure, arrhythmia, and endocarditis. Mitral valve stenosis is defined as the narrowing of the mitral valve apparatus; the most common cause is rheumatic heart disease where the leaflets become thickened and rigid, and the chordae tendinae become shortened due to fibrosis.

Secondary or functional MR when the leaflets and the mitral annulus apparatus are normal, but there is an abnormality of the ventricular wall, that results in a dysfunction between the wall motion, the papillary muscles and the annulus increasing their distance and resulting in the restriction of the leaflet motion.

Most of the mitral regurgitation cases are associated with structural issues causing dyspnea, fatigue, and orthopnea that, in severe cases, can ultimately lead to heart failure with pulmonary congestion and edema.

Once the severity of the valve defect has been established, an indication whether surgical intervention for repair or replacement is needed. The ideal time of intervention would be before an irreversible compromise of the ventricular function is reached. Indeed, an operation performed early, especially if it consists of a repair, involves a low operative risk and allows the patient a quality and life expectancy not different from the normal population. The advantages of repair over replacement include improvements in survival, lower perioperative mortality and better preservation of the post-operative ejection fraction.

When valvular repair is not considered feasible, mitral valve replacement with preservation of the subvalvular structures is considered the next option.

1.3. Mitral Regurgitation Repair

The past decade has seen advances in all forms of cardiovascular care, and this is especially true with SHDs. Increased recognition of the diseases and patho-physiologic mechanisms underlying these diseases is due to advanced imaging techniques, that elucidate more finely anatomic abnormalities [22]. Catheter-based techniques and imaging devices have each contributed to improved diagnosis and treatment of SHDs. As a result, Structural Intervention Cardiology (SIC) is emerging as its own medical specialty that focuses on therapeutic interventions for SHDs that do not require surgery, but a mini-invasive intervention with a catheter-based approach, allowing repair or replacement devices in the heart [26].

1.3.1. Structural Intervention Cardiology

The traditional way of performing mitral valve replacement or repair is by open-chest surgery. This is known as sternotomy and it is still used for some cardiac surgery procedures, as it gives the surgeon very wide access to perform the operation. The procedure is performed under a general anaesthetic and usually takes between two to three hours. After the operation, it can take the patient an average of two to three months to recover

from this type of operation. The disadvantages of this kind of procedure are straightforward, as they show higher pain and major risks for the patients, such as infection, heart attack, kidney failure, and stroke [42]. Furthermore, slower recovery and longer hospitalization stays raise healthcare costs [11].

Alfieri et al. [19] first described the surgical repair of anterior mitral valve leaflet prolapse using an edge-to-edge technique. This technique is performed through a conventional median sternotomy in which the free edges of the mitral leaflets are approximated in correspondence of the site of the regurgitant jet in order to correct mitral regurgitation without producing stenosis (Figure 1.4).

Since the Alfieri repair is acting at the leaflet level, it can be applied independently of the underlying mechanism of MR so it is the only therapy that can be effective both for degenerative and functional MR [5].

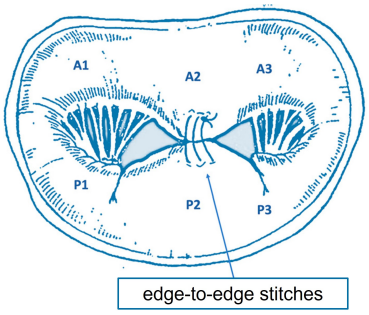

Figure 1.4: *Alfieri's edge-to-edge repair consisting in the approximation of the free edges of the mitral leaflets in correspondence of the site of the regurgitant jet through stitches.*

On the other hand, minimally invasive mitral valve repair refers to operation performed via incisions other than full sternotomy. These approaches include partial sternotomy, mini-thoracotomy, percutaneous access, and robotic surgery. Patients perceive minimally invasive approaches to be less traumatic, which is an important consideration for high-risk patients who require repair of severe mitral valve regurgitation but cannot tolerate open-chest surgery. Hence, SIC procedures had significant advances, developing less-invasive Transcatheter Mitral Valve repair (TMVr) techniques to mimic surgical edge-to-edge therapy of MR correction through a percutaneous approach. SIC is today an established medical field and, with adequate training, the majority of today's mitral valve procedures can be performed safely [39].

Although increasingly popular, SIC procedures are characterized by costly requirements:

- A dedicated room called the cardiac catheterization laboratory (CATH-lab) that

houses a C-arm and a sonographer to acquire Real-Time 3D Transesophageal Echocardiography images (RT3DTEE) through a probe mounted at the tip of a catheter (Figure 1.5).

- Two leading operators, the interventionist, who commands every small movement of the catheter at every step of the operation, and the echocardiographist who handles the RT3DTEE sonographer.

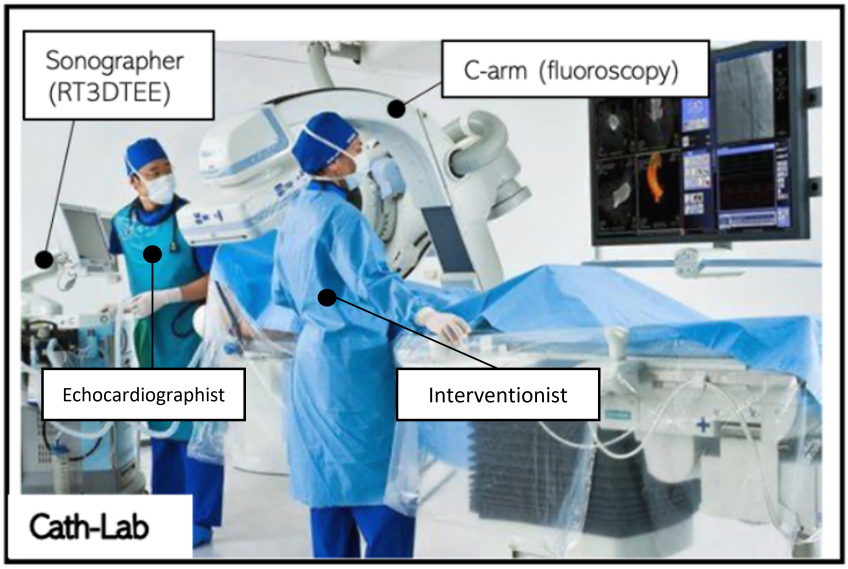

Figure 1.5: *CATH-lab with the two operators and imaging devices: the C-arm that encompasses a portion of the surgical table and acquires fluoroscopic images through the emission of X-rays and the RT3DTEE sonographer inserted into the patient's esophagus to visualise the heart.*

Thus, percutaneous SHD treatment is still hampered by important hurdles, mainly originating from the lack of direct vision and access to the implant site. Indeed, coordination between the interventionist and the echocardiographist is crucial. In addition, surgery success relies heavily on image-based guidance (Figure 1.6) and the operator's expertise.

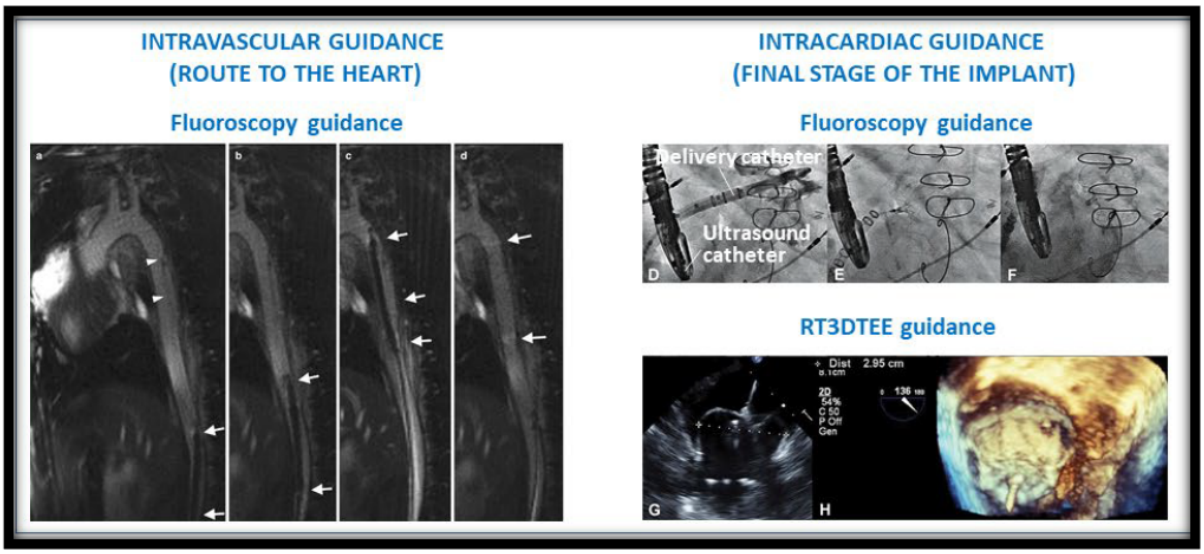

Figure 1.6: *Image-based guidance. On the left: intravascular example of fluoroscopy used for monitoring the route of the catheter. On the right: intracardiac imaging modalities used for driving catheter and device positioning; fluoroscopy allows for the 2D vision of the catheter and of the nearby trans-esophageal ultrasound catheter; real-time 3D trans-esophageal echocardiography allows for 2D measurements (left) and for the 3D rendering of the anatomy and of the device (right).*

Currently, different devices have been designed and used for treating mitral regurgitation through minimally-invasive approach, and will be briefly described.

PASCAL™

The PASCAL™ Precision Transcatheter Valve Repair System (Edwards Lifesciences) received CE mark approval for the treatment of MR and was introduced in 2019 after showing acceptable outcomes in the CLASP studies [40, 62] in patient populations with functional, degenerative, and mixed MR. The device system includes a delivery system and a permanent implant. The delivery system allows three independent catheter movements in different planes, allowing for height compensation in cases of suboptimal trans-septal puncturing, delivery system control, and implant positioning and orienting (Figure 1.7 A). The PASCAL™ implant looks and functions like a clip. It consists of two paddles, two clasps and a central nitinol spacer: the two paddles promote leaflet approximation, while the two clasps allow for independent leaflet capture and adjustment of leaflet against the spacer to ensure a low and uniform pressure distribution on the valve tissue (Figure 1.7 B-D). The insertion is carried out using the delivery catheter through the femoral vein and guided through the blood vessel and a trans-septal puncture to the left side of the

heart. Once in the heart, the clip is used for grasping the two valve leaflets, reducing the blood backflow. After the clip is in place, it is disconnected from the delivery catheter and then the delivery catheter is removed from the body (Figure 1.7 E).

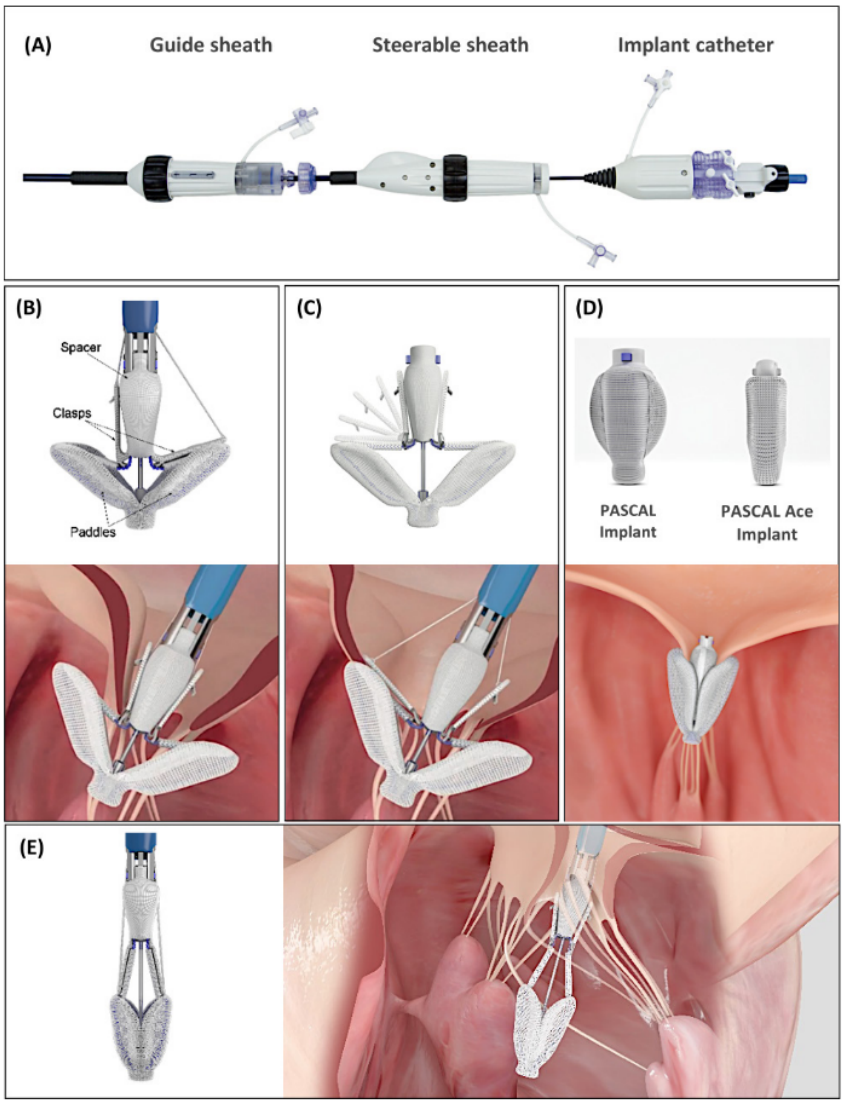

Figure 1.7: *PASCAL Transcatheter Valve Repair System. (A) Components of the PASCA™Łdelivery system; (B) PASCAL™ implants made of two paddles, two clasps and a central spacer; (C) Independent leaflet capture; (D) The newest generation PASCAL Ace™ implant; (E) PASCAL™ device implant procedure. Images courtesy of and provided by Edwards Lifesciences.*

Although the procedural and clinical success rates were 92% and 87% for functional and degenerative MR respectively, it has not seen the same diffusion or adoption in daily clinical practice as the MitraClip™ system [18].

MitraClip™

In 2008, the Mitraclip™ system (Abbott Vascular, CA, USA) received CE mark approval for the treatment of MR, and its use has steadily increased since then. It also received Food and Drug Administration approval for degenerative and functional MR in 2013 and 2019, respectively. Today, it has been implanted in more than 1,000,000 patients in over 50 countries and is the only TMVr therapy to complete prospective trials comparing the device to conventional mitral valve surgery. The MitraClip™ system consists of a Steerable Guide Catheter and a Clip Delivery System, which includes the detachable Clip implant (Figure 1.8 A).

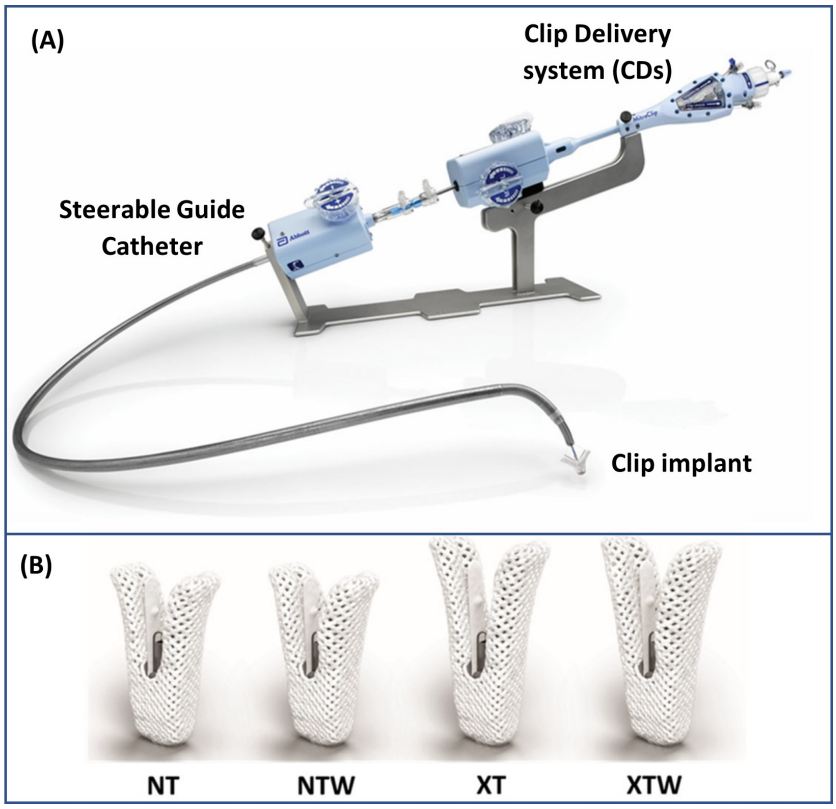

Figure 1.8: *Mitraclip™ system: (A) Clip Delivery System and Steerable Guide Catheter for Clip implant delivery; (B) Clip implant sizes for patient-tailored TMVr.*

The Steerable Guide and Clip Delivery System allow manoeuvring the clip in different planes intending to assist the operator in the treatment of challenging anatomies. In particular, through a set of knobs, it is possible to act on the Steerable Guide and Clip Delivery System to obtain catheters' bending into two perpendicular planes, named Medial-Lateral (ML) and Anterior-Posterior (AP). These actions on the MitraClip™ system allows to perform the edge-to-edge valve repair through a "V shaped" clip made of

cobalt–chromium alloy covered in polyester fabric whose size can be chosen among four types (Figure 1.8 B) offering more options for patient-tailored TMVr. MitraClip™ insertion procedure is performed by pushing the Delivery Catheter through the femoral vein up to the right side of the heart, then the left side is reached trough a trans-septal puncture. The clip consists of two arms that are opened and closed by control mechanisms on the Clip Delivery System and two 'grippers' that match up to each arm and help stabilising the leaflets as they are captured during closure of the clip arms. Once the left atrium is reached, leaflet tissue is secured between the arms and each side of the gripper, and the clip is then closed and locked to maintain leaflet coaptation (Figure 1.9). Prior to clip deployment, a haemodynamic assessment is performed. Pressure gradients are assessed to ensure there is no clip-induced mitral stenosis. If needed, the interventionist may also place a second or third clip to optimise MR reduction.

Figure 1.9: *Mitraclip™ intra-cardiac procedure. From left to right: insertion through trans-septal puncture; leaflets gripping; clip deployment and catheter removal. Image courtesy of and provided by [18].*

Both transcatheter approaches previously described are performed under general anaesthesia using fluoroscopy and Trans-Esophageal Echography (TEE) guidance. Although they have been proved to be as effective as open-chest surgeries [34] [4] and are now being gradually expanded from high risk to moderate and even low risk patients [34], complexities of percutaneous SHDs treatments persist. Indeed, the current paradigm of SHD percutaneous treatments consists in a completely manual procedure with many challenges:

- The targeted heart structures are dynamic, anatomically complex, and delicate. The usual 2D picture rendering is challenging to comprehend, thus relying exclusively on fluoroscopy and RT3DTEE for guidance considerably increases the difficulty of exact positioning the implant at the correct site;
- Fluoroscopy X-ray exposes both patients and operators to harmful X-ray radiation. In addition, nephrotoxic contrast chemicals, that are injected into patients to increase image quality, can also cause major issues as renal failure [24];

- Complex sets of well coordinated steering motions are needed to target a specific point while avoiding delicate anatomical regions. Navigation accuracy is severely impacted by external disturbances like pulsatile flow or contact with tissue. Because of the slack, friction, and compliance in the path leading to the heart, the relationship between the input (proximal steering motions) and the desired output (positioning of the catheter distal end) is very non-linear and unpredictable.

Therefore, the critical aspects of manual TMVr procedure can be summarized in the following: i) requirement of two main operators, ii) dependency on their dexterity and coordination, iii) huge dependency on the prior experience of the interventionists, and iv) exposition of patients and operators to relevant amounts of X-ray radiations.

1.3.2. Structural Intervention Cardiology Robotic Approach

Robotic cardiac catheterization approach emerged when heart surgery has been performed through very small incisions in the chest with the help of instruments and robot-controlled tools. Current applications of robotic telemanipulation include two major fields of cardiac catheterization: mitral valve surgery and coronary artery re-vascularisation/ablation, all showing great outcomes [29, 54]. Commercial robotic systems have been developed; among these devices, the Magellan™ and the Sensei™ X from Hansen Medical (Mountain View, CA, USA), and the CorPath GRX from Corindus Vascular Robotics Inc. (Waltham, MA, USA) can be found [47]. Recent advances in the field of robotics have seen developments in the concept of automation: robotic systems performing surgical procedures autonomously assisting the access to the organ, heart manipulation and compensation for heart tissue motion [12]. As traditional minimally-invasive surgeries the main advantage of robotic cardiac catheterization over open-heart surgery is that it is less traumatic and painful for patients, with a reduced fluoroscopy radiation and risk of rehospitalization maintaining the same surgical efficacy [64]. However, there are still barriers to the adoption of robotic cardiac procedures including:

- lack of recognised training and steeper operator's learning curve [31];
- lack of haptic feedback that may result in longer operating times;
- lack of a demonstrated superiority of robotic procedures over traditional minimally invasive ones;
- need of larger infrastructures and higher costs which are approximately 1.5 million for each unit, with annual service costs of approximately 112.000 per year and extra cost for the disposable supply [55].

At present state, the potential of robot-assisted interventions has only been tested in clinical studies on relatively small patient cohorts; however, all of them strongly suggest that robotic systems effectively reduce radiation exposure for operators and improving device deployment precision [65].

This is the reason why the European ARTERY project was born: propose an innovative product to advance state of the art on robotic-assisted cardiac catheterization of mitral valve repair.

1.3.3. ARTERY Project

As mentioned in previous Section 1.3.2, although increasingly popular, percutaneous approaches are highly technical, non-ergonomic and typically involve a steep learning curve, and surgery success is connected to the operator's experience. In particular, throughout the TMVr process the operators will not have a direct view of either the catheter or the targeted heart parts, and will be guided through intra-operative clinical imaging, where X-ray fluoroscopy and RT3DTEE are performed manually by an echocardiographist. Navigating through these images is far from intuitive and extremely challenging with the continuous risk of using the device incorrectly with higher probability of human error. As a result, only a very small number of centres of excellence can offer this life-saving percutaneous procedure. To date, MitraClip™ system, is the most successful device used in these valve repair procedures. The ARTERY project aims to fully exploits the potential of this procedure in order to accelerate percutaneous treatment of SHDs while also developing a procedure that is easier to learn and perform, safer, and radiation-free. ARTERY will design, build, and benchmark a completely novel variable/shared autonomy robotic platform for performing life-saving percutaneous SHD procedures. To reach this goal, the complete system will comprehend three parts:

Bootstrapping: from the available CT scan data of the patient together with the data coming from the Fiber Bragg Grating and Electromagnetic Sensors, the computational model of vessel and heart is obtained to provide a fully immersive augmented reality interface through which the operator can monitor the catheter's path without the need for radiation-based imaging;

Intravascular: once the desired target is selected virtually on the valve, the optimal path is generated from the Path Planner Module, then the actuation of the robotic system can be executed. AI algorithms will autonomously identify optimal trajectories and safer navigation paths that the catheter has to follow to reach the point. The autonomous catheter moves its distal section to align with the path planner's

trajectory. As a result, AI and control algorithms make catheter navigation a simple task, allowing the surgeon to monitor in real-time the catheter through sensors that provide information on the distal end's pose and force, with a reconstruction of vessel wall deformations caused by catheter movement;

Intracardiac: during the final stage of the surgical procedure, the catheter is directed towards the target point by the Inverse Kinematic Controller Module. A closed-loop control algorithm is used for correcting the catheter's pose. At the same time, the RT3DTEE robotic probe and Sonographer, will follow the tip position of the catheter so that a the mitral valve segmentation can be performed to provide the surgeon with a clear view of the relevant anatomical area.

All the constitutional parts of the ARTERY project are represented in Figure 1.10.

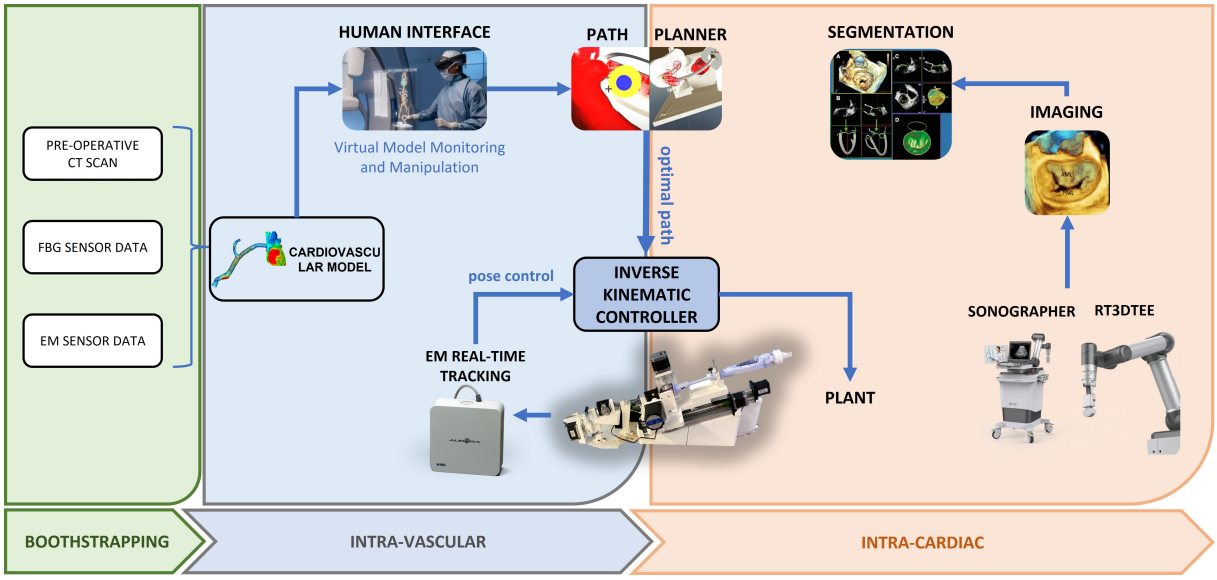

Figure 1.10: *Global Schema of integration of the different modules of ARTERY project. From the available data of the CT scan of the patient and the data coming from the Fiber Bragg Grating and electromagnetic sensors, the computational vessel's model is obtained. Subsequently, a 3D holographic interface is generated and the surgeon can interact with the hologram by inspecting the modelled anatomy and grabbing the target point of the intervention. This point is sent to the path planning module that computes the optimal path and passes the trajectory to the Inverse Kinematic Controller. The latter. produces as output the variable for controlling the actuation plant. An additional closed-loop pose control is inserted exploiting the electromagnetic tracking system. Only during the intra-cardiac phase of the intervention, the module of segmentation and recognition of the mitral valve is activated to provide to the surgeon a clear vision of the anatomical region of interest. Image adapted from [35].*

This innovative solution will pave the way towards a scenario envisioned in ten years from now: in the future, SHDs percutaneous treatments will be performed by autonomous robots, with minimal mental workload for the interventionists and maximal safety for physicians and patients. With the absence of damaging radiation and the intuitiveness of operation, the new percutaneous approach could become the gold standard of TMVr procedures, offering a safer and reliable outcome, gradually abandoning open chest surgery.

This thesis is structured as follows:

Chapter 1 introduced the clinical background and ARTERY project.

Chapter 2 analyses the first robotic MC prototype and the state-of-the-art of current continuum robot control strategies.

Chapter 3 presents a new robotic actuation prototype for the tendon-driven MitraClip™ system and explains the developed control algorithm.

Chapter 4 describes the experimental set-up and protocols to obtain the results.

Chapter 5 presents the results obtained to determine the system's quality.

Chapter 6 discusses the obtained results.

Chapter 7 conclusions of the work, exploring its limitations and possible future developments.

2 | State of The Art

The upcoming chapter is going to be divided into two sections. The first part will describe the working principle of the manual MitraClip™ (MC) system and will go through the first ARTERY project milestone that has been reached for its robotic actuation. The second part will cover different state-of-the-art control methods applied to soft/continuum robots.

2.1. MitraClip™ System

The MC system comprises two main components: the Steerable Guide System and the Clip Delivery System (Figure 2.1).

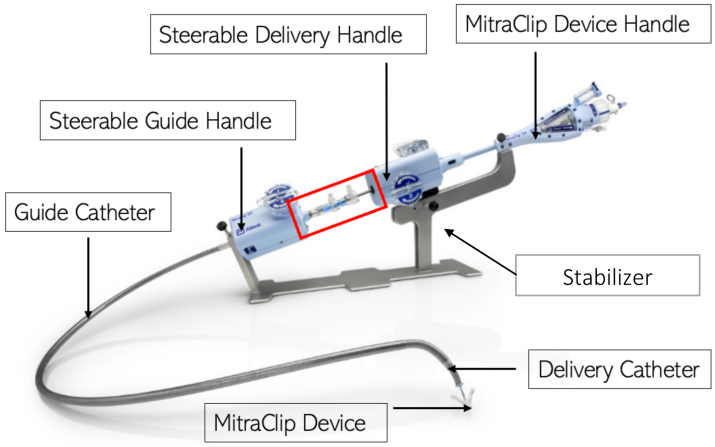

Figure 2.1: *Overview of the MC system and main components devoted to the manual actuation: the three knobs on the two handles, i.e. Steerable Guide Handle and Steerable Delivery Handle, are rotated to obtain the bending of the Delivery Catheter and the Guide Catheter. The advancement of the Steerable Delivery Catheter inside the Guide Catheter takes place in the highlighted area by pushing one catheter inside the other. Image courtesy of [35].*

The actuation is performed manually by the operators through independent motions of the two parts using the following components:

- Steerable Delivery handle to perform insertion/extrusion of the Delivery Catheter inside Guide Catheter and bending in two different planes (Figure 2.2 A);
- Device Handle in order to further insert MC implant in between valvular leaflet, adjusting its arms independently to any position between fully open, fully inverted, and fully closed, with a maximum angle of 120°. The grippers can be raised and lowered indefinitely to allow the MC Device to grasp and approximate the mitral valve leaflets. Eventually, the clip body can be detached from the Delivery Catheter to complete the TMVr procedure (Figure 2.2 B).
- Steerable Guide Handle in order to perform Guide Catheter rotation and bending in one plane (Figure 2.2 C).

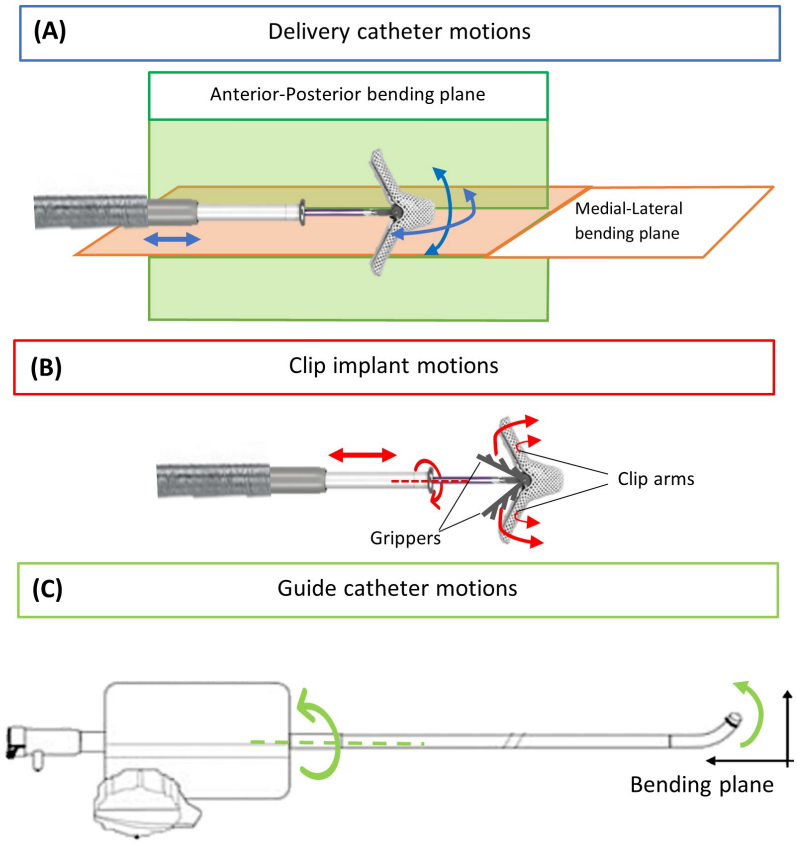

Figure 2.2: *MC system possible motions: (A) Delivery Catheter insertion and bending in Anterior-Posterior and Medial-Lateral planes; (B) Clip implant insertion, rotation and independent opening/closing of clips' arms and grippers; (C) Guide catheter rotation and bending (Medial-Lateral plane).*

To perform the TMVr procedure, the Steerable Guide Catheter is introduced inside the femoral vein, then after the trans-septal puncture, the Clip Delivery System is inserted

in the Guide up to the left side of the heart. The complete procedure of the implantation of the clip is summarized in Figure 2.3.

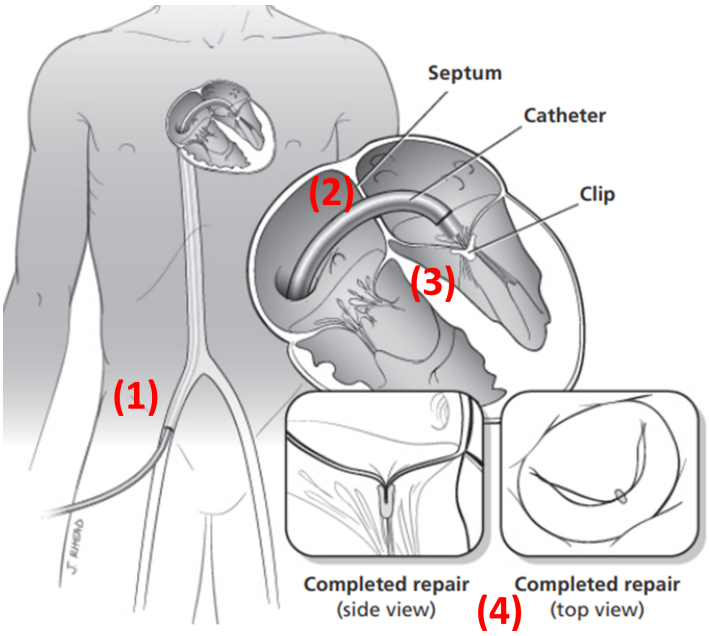

Figure 2.3: *TMVr procedure: (1) The Steerable Guide Catheter is introduced into superior vena cava with the support of a 0.032 Teflon J wire; (2) it is advanced until it reaches the fossa ovalis in the septum. The puncture, performed by the use of a needle and under TEE and fluoroscopy monitoring, is made such that its distance from the mitral valve is greater than 3.5 cm; in this way, the behave of the MC Device is predictable; (3) The Delivery Catheter is pushed inside the Guide, after the extraction of the needle, and the MC Device is correctly oriented upon the mitral valve and then inserted in the left ventricle to grasp the leaflets; (4) The clip is detached and the catheter is removed finalizing the procedure.*

Other accessories used in conjunction with the MC System are: 1) a Stabilizer, 2) a Lift, 3) a Support Plate. The Stabilizer is provided separately as a non-sterile reusable device and must be cleaned and sterilized prior to each use. It is used on the sterile field to support and position the Steerable Guide Catheter and Clip Delivery System at 20° during the procedure to facilitate the insertion and manoeuvrability (Figure 2.1). The Lift and Support Plate are provided separately as non-sterile reusable devices and must be cleaned prior to each use. Their role is to provide a stable platform for the Stabilizer and MC System during the procedure.

2.2. First Robotic System Prototype

The MC system is a tendon-driven actuated device (Figure 2.4), the Guide and the Delivery Catheter are guided and manoeuvred manually thanks to the use of knobs that are located on the Steerable Guide Handle and the Steerable Delivery Handle, respectively.

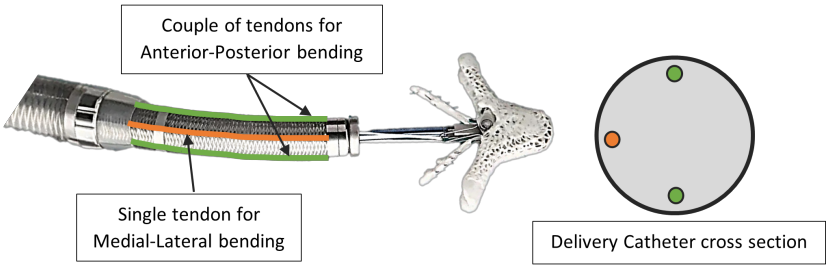

Figure 2.4: *Delivery Catheter Distal End. Left: schematic representation of the tendons used for moving the Steerable Delivery Catheter into Anterior-Posterior (AP) and Medial-Lateral (ML) planes. Right: Delivery Catheter cross-section with highlighted tendons.*

For the first robotic system prototype proposed in [35], the knobs on the two handles were substituted with electrical stepper motors, while the manual translation of the system was accomplished by exploiting a linear electro-mechanical motor for advancing the Delivery Catheter inside the Steerable Guide. Hence, in [35] the system proposed is a catheter actuation plant with 3 Degrees of Freedom (DoFs): ML bending in the frontal plane, AP bending in the sagittal plane, and translation insertion inside the Steerable Guide. Both the Steerable Guide Handle and the Steerable Delivery Handle have been re-designed in Solidworks® environment in order to house the new motorized components (Figure 2.5).

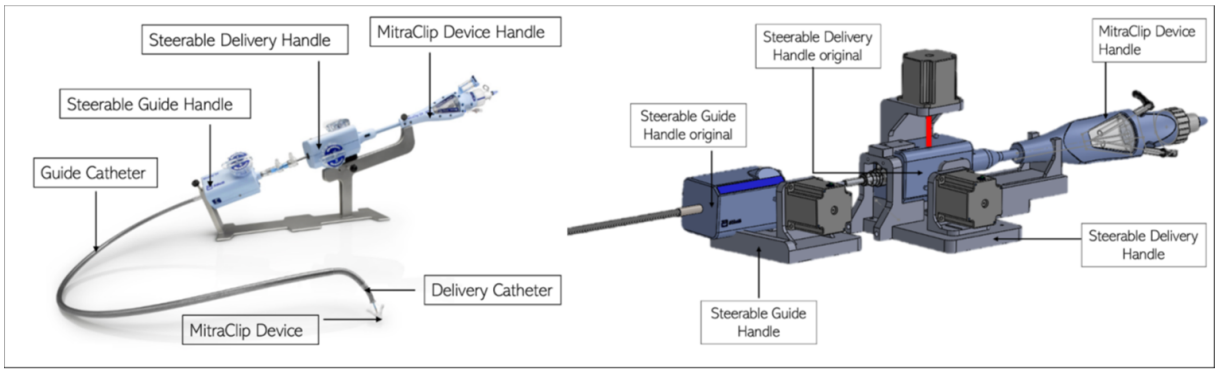

Figure 2.5: *Comparison of the commercially available MitraClip™ system's with [35] proposed design.*

For the realization of this prototype, an Ultimaker s3 3D printer was used with Acryloni-

trile Butadiene Styrene (ABS). The choice of this material was justified in [35] so that the new support could weight much less than the maximum weight that the carriage of the linear actuator can transport and, at the same time, it could easily support the weight of the motors and the remaining parts of the MC. The electrical components chosen for the real system were:

- Nema 23 Stepper motors (JoyNano) with control precision (1.8°±0.09° for each step) and maximum holding torque (1.26 Nm);
- Nema 17 Bipolar Stepper Motor (Sainsmart) connected to a 300 mm linear guide with precision of ±0,03 mm maximum axial load of 10 kg;
- a DM556 driver (Jadeshay) for each motor, with eight current levels with a resolution of 0.5 A;
- Arduino Uno board controller;
- 24V power supply.

The complete robotic system realized in [35] is shown in Figure 2.6.

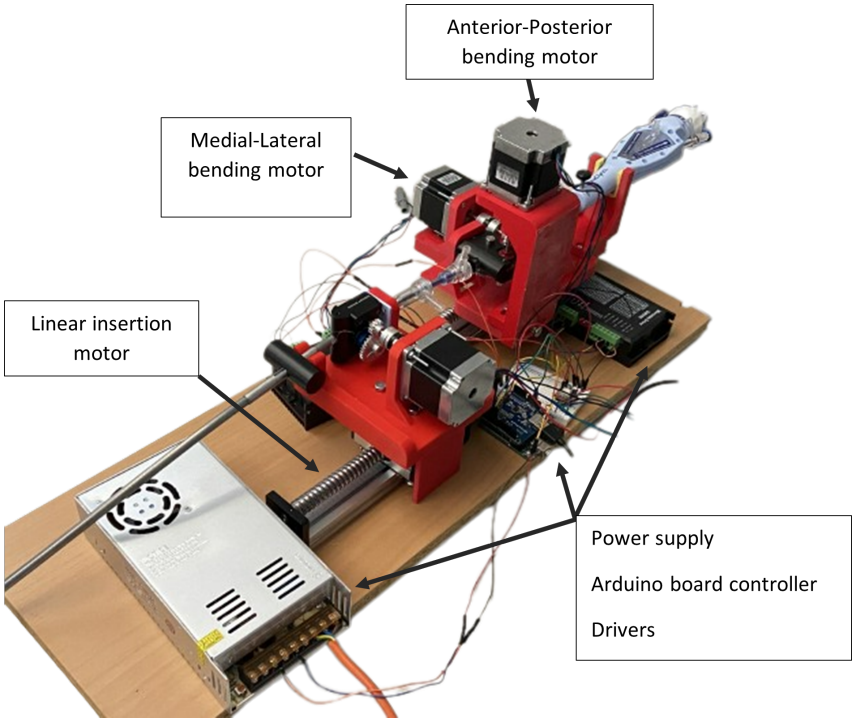

Figure 2.6: *Complete system realized in [35] with its electrical components.*

Although this first prototype holds the ability to move in forward direction to mimic the manual insertion, and to bend in the AP and ML planes, which are fundamental to

manoeuvrer the Delivery Catheter inside the heart chamber, it still lacks of the following technical and clinical requirements:

1. System inclination of 20° traditionally achieved by the Stabilizer, which is considered clinically relevant for an optimal procedure performance;
2. Mitraclip™ Device Handle mechanism to control tip insertion, positioning and leaflet grasping as described in Figure 2.2 B;
3. Steerable Guide Handle rotation and bending motions (Figure 2.2 C).

2.3. Tendon-Driven Continuum Robot Control

2.3.1. Continuum Robot

Steerable catheters for minimally invasive surgery as the MC system belong to the subfield of robotics of continuum manipulators. Continuum robots have a fundamentally different structure than conventional ones composed of discrete rigid links connected by joints. When a robot has more DoFs than necessary to execute a task, it is said to be redundant or hyper-redundant. In the limit, as the number of joints approaches infinity (and the link's length approaches zero), the robot becomes what is known as a continuum robot [51]. Continuum manipulators are mechanisms without rigid links but with elastic structures that can bend continuously. A subdomain of continuum manipulators, called "soft robotic manipulators", has rapidly grown in the past decade. These manipulators are made of soft materials, such as silicone, and are inspired by boneless organisms that exhibit dexterous manipulation in cluttered environments (Figure 2.7). Soft robotic manipulators simplify complex tasks, offer a low-cost alternative to numerous robotic applications, and facilitate safe human-robot interaction. The demand for them is rapidly increasing in industrial, surgical, and assistive applications due to their characteristics [25].

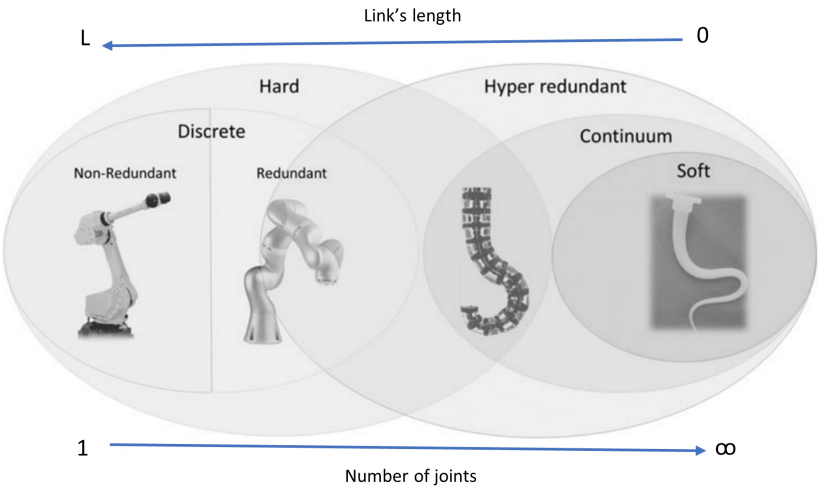

Figure 2.7: *From left to right: evolution of rigid-link manipulators from discrete mechanisms to bio-inspired continuum soft robotic manipulators as the links' lenght approaches zero and number of joints becomes infinite. Adapted from [25].*

2.3.2. Tendon-Driven Actuation

Wire- or tendon-driven robots, whose joints are driven through a wire, have been discussed extensively in the field of robotics [8, 33, 41, 48, 57]. In the tendon-driven mechanism, multiple joints are driven simultaneously by pulling a wire that passes through points, e.g., pulleys attached to links (Figure 2.8).

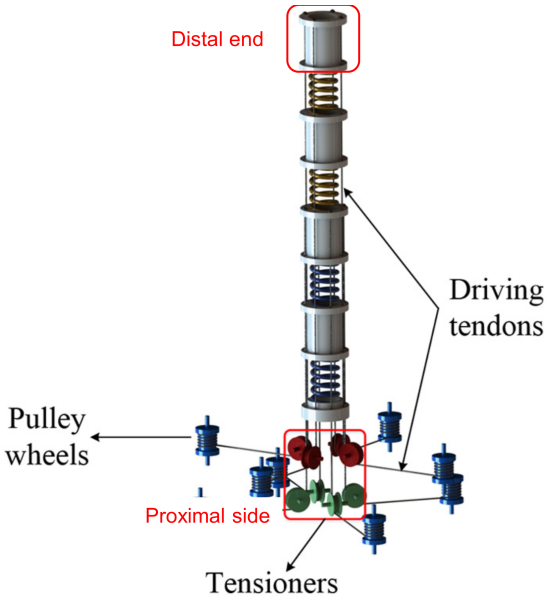

Figure 2.8: *Components and arrangement of tendon driven system made of multiple joints driven by pulling wires that pass through pulleys and tensioners. Adapted from [33].*

In typical minimally invasive cardiovascular procedures, interventionists use a combination of guide-wires, sheaths, and catheters. They push, pull, and rotate these devices proximally and manually through the vascular system up to the heart. The vast majority of steerable catheters used in clinics, such as the MC system, are outfitted with cables that run from control knobs on the catheter's proximal side to the catheter's distal end. As a direct consequence of knob handling, the cables are pulled or released, resulting in distal bending. Since the cables are in constant contact with their housing, they require significant forces to pull them through the friction, causing the cables to temporarily stick and then slip, thus making it difficult to precisely control the distal tip position. To avoid large overshoots, the operator will generally slow down his/her movement, and the actions on the knobs will be performed sequentially to minimize those errors [1].

As a general concept, the actuation performed to this kind of continuum robot is simply linked to the cables that are part of the structure. Thus, the tendon/cable actuation is easy to realize and relatively easy to control [13], since the possible control variables are the tendons' tension that has to be applied or the amount of tendons' length that has to be pulled/released. On the other hand, controlling continuum robots is an extremely challenging task due to the non-linearity of the materials from which soft manipulators are build with, that generate phenomena like bending, extension, contraction, torsion, and give rise to essentially infinite DoFs motions, thus rising the computational complexity in case of model-based approaches.

2.3.3. Continuum Robot Control Strategies

Modelling soft robots requires different strategies than those used for rigid robots due to significant differences in their movements. While the movement of rigid robots is determined by the rotation and bending of each joint connected by rigid bodies, soft robots can deform at any point along their soft materials, giving them an infinite range of DoF including bending, extension, contraction, and torsion. Another important difference is that soft materials have non-linear and time-dependent properties, making it challenging to model and use model-based approaches for control [61]. Furthermore, in contrast to rigid robots, which typically operate in well-defined environments, soft robots are intended to operate in unstructured scenarios.

Different control strategies for soft robotic manipulators have been applied and analysed in the past few years. Soft robot control techniques can be categorized mainly into two types of modelling approach:

Model-based controllers: based on models derived from analytical kinematic methods.

Analytical models based on physics or mathematics simplify the number of DoFs in a robot, but are limited in accuracy due to assumptions made about the robot's structure and actuation mechanism. Only those models with a strong background in physics can develop strong analytical models. Additionally, the controlling approaches for soft robot's movements depends on: static/kinematic models where the dynamics of the soft robot are neglected, and dynamic model that, as the name suggests, takes the robot's dynamics into account (Figure 2.9);

Model-free controllers: based on data-driven techniques. The main advantage over their model-based counterpart is that they don't require defining the parameters that map the task space to the operating space of choice. The downside is that it is impossible to establish convergence of the controller or even a stability analysis due to the lack of a clearly parametrized model.

In recent years, a third category has also emerged that combines the two previously mentioned approaches, creating hybrid controllers [3, 49, 56].

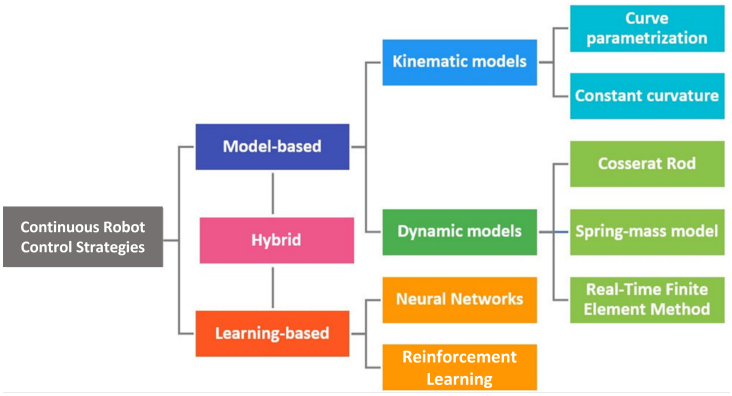

Figure 2.9: *Continuum robot control strategies schematic. Adapted from [38].*

Lastly, another controlling strategy classification can be made by differentiating between open-loop and closed-loop control methods.

Open-loop control: involves predicting movement based on knowledge of the robot and the space in which it is operating [28]. Open-loop control lacks feedback, making it unsuitable for situations where the robot interacts with unknown environments or objects. Small errors in time-varying materials properties can result in significant errors in sequential tasks, thus open-loop control is typically used for short or repetitive tasks.

Closed-loop control: relies on sensors to provide feedback about the deformation state of the actuators and their contact state with the surrounding environment. Closed-

loop control is necessary when the environment or task are uncertain. In robotics, closed-loop control has two levels (Figure 2.10): the first controls the deformation state of individual actuators, and the second controls the overall robot body. The first level focuses on monitoring actuator mechanisms, while the second level includes the kinematics and dynamics of the robot body. The primary function of the second-level control loop is to connect the configuration or task space to the joint space outputs, as referenced in [61].

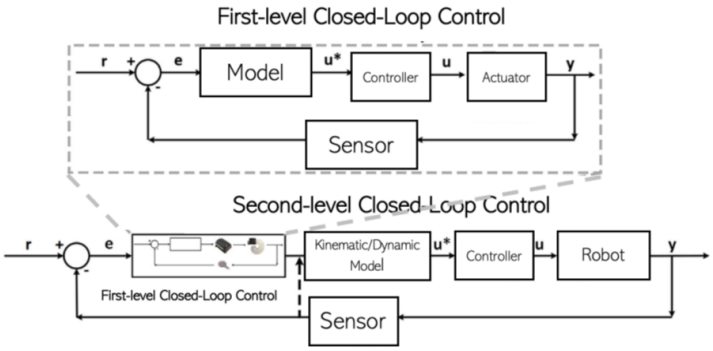

Figure 2.10: *First and Second level Closed-Loop control schemas. The first-level Closed-Loop adds a sensor to the feedback branch to compare actuation y with the desired one r. The error is fed to the model, which tries to minimize it. To this first loop can be added the Second-level Closed-Loop in which another feedback and kinematic/dynamic models of the robot are introduced for further correction. Adapted from [61].*

2.3.3.A. Model-Based Control Strategies

Currently, the most commonly used approach for controlling continuum/soft robots is through model-based static controllers, as many surveys report [20, 25, 28, 61]. These controllers typically rely on the Pseudo Ribgid Body (PRB, fig 2.11 a) and Constant Curvature (CC fig 2.11 b) approximations due to their lower computational expense and design specificity with respect to more complex models [53] A slightly advanced model is the Piecewise Constant Curvature (PCC), which divides the robot's path into segments, where each segment has a constant curvature. Despite the approximations, the CC/PCC model is still regarded as a trustworthy and simple method for controlling uniform, low-mass manipulators because it has been validated for many soft robots [28]. On the other hand, the Variable Curvature (VC) model allows for a more flexible motion path by allowing the curvature to vary continuously along the whole robot. More complex method, such as the Cosserat rod model (CR, fig 2.11 c), is also used. It models the robot's kinematics and dynamics using a set of differential equations that describe the

deformation of each small segment of the robot, taking into account both the internal structure of the rod (cross-sectional shape, distribution of material properties, etc.), in combination with the effects of the rod's environment (friction, gravity, and fluid flow), allowing for a more accurate representation of the rod's behaviour and making it suitable for modelling rods in complex environments, such as biological systems [50].

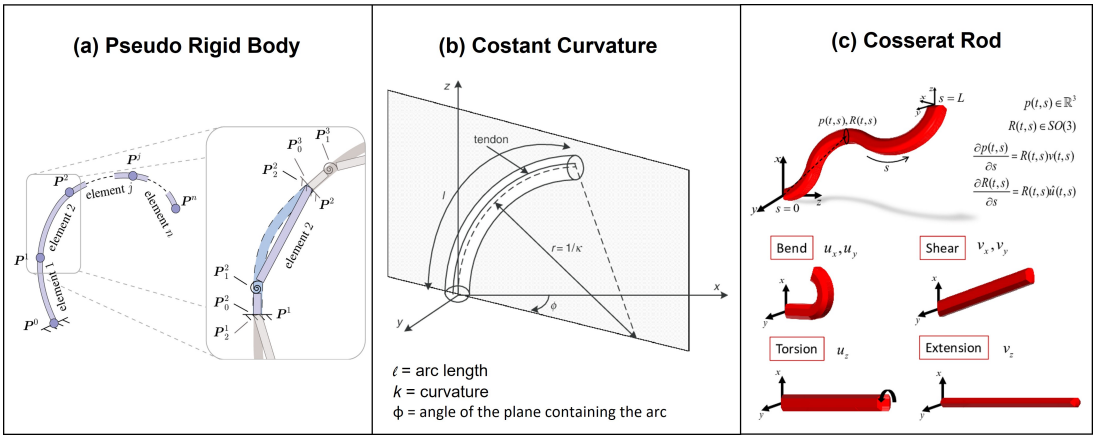

Figure 2.11: *Soft/Continuum robot's models: (a) Pseudo Rigid Body describe the motion and force the soft robot using a rigid-body mechanism with equivalent behaviour for small segmented portions along its whole length; (b) Constant Curvature describes soft robot sectional curvature as constant at every point and for every two-dimensional tangent plane at that point; (c) Cosserat Rod formulates a set of governing partial differential equations of motion in terms of the displacements and angular variables, describing the non-planar, non-linear dynamics of an extensional rod.*

In terms of controller configuration, closed-loop controllers in configuration space or joint space offer greater stability and speed but may not guarantee error convergence without a perfect forward model. On the other hand, closed-loop task space controllers theoretically provide the best accuracy [28].

As an example, in [14, 37, 59] open-loop control strategies based on a combination of geometric and physical models of the manipulator's behaviour are described, which take into account the non-linear and complex behaviour of soft robots and provide a way to optimize the control input to achieve desired manipulator motion. In this case, since the proposed control strategies are based on an open-loop approach, they do not take into account any feedback from the environment or the manipulator itself. Although the physical and geometric models used for designing the control strategy are accurate representations of the manipulator's behaviour, in practice there are errors and uncertainties in these models that affect the performance of the control.

In [33, 45] model-based approaches on the assumption of a constant curvature (CC) model have been proposed, and a position closed-loop Proportional-Integrative-Derivative (PID) controller is then developed (Figure 2.12 B). With the same assumption of CC model, the authors in [30] proposed instead a Model Reference Predictive Adaptive Control which is a feedback control method that uses a reference model to predict the behaviour of the controlled system and adjust the control inputs accordingly (Figure 2.12 C). However, since the CC is a simplified model of the robot's kinematics, it assumes the robot as continuous, homogeneous, and with an isotropic structure. This may not accurately capture the behaviour of the robot in all situations, especially when dealing with more complex environments where external factors have a high influence on the control performance.

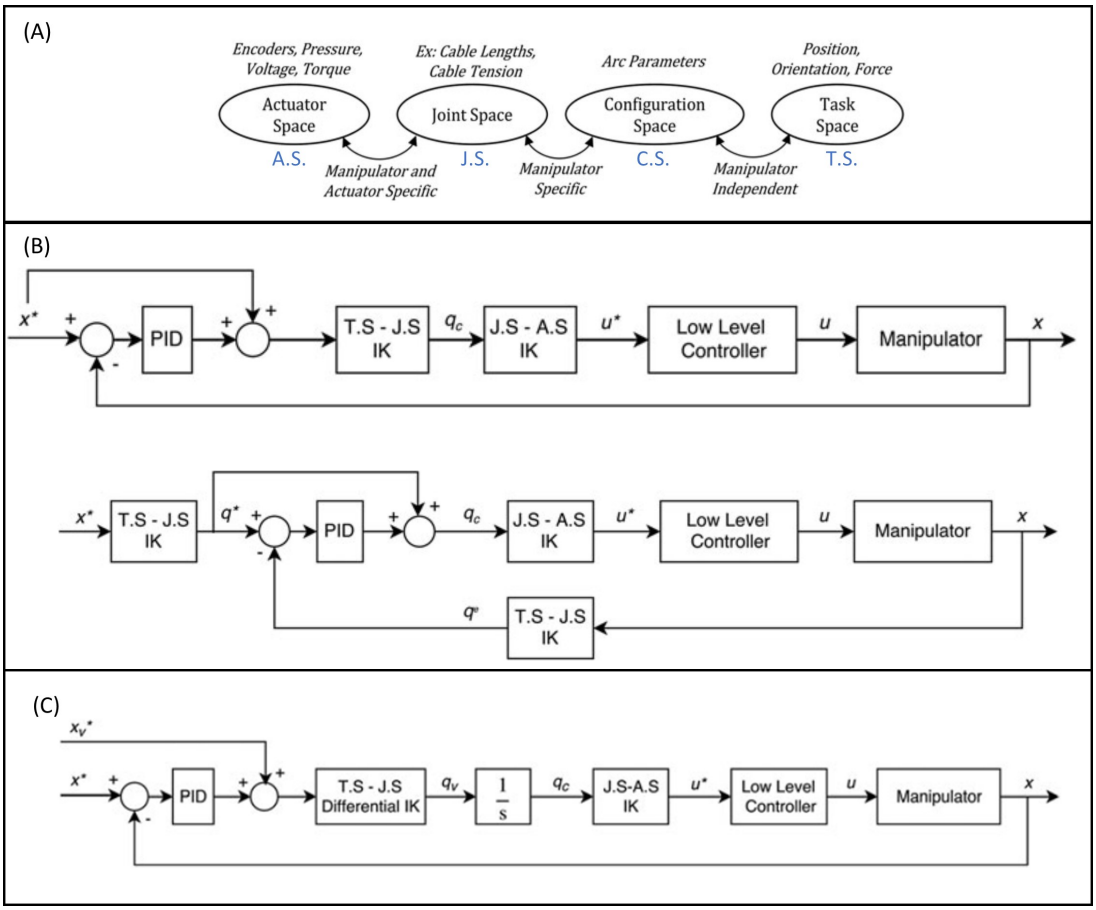

Figure 2.12: *State-of-the-art model-based continuum robot's control: (A) Manipulator's space and parameters definition ; (B) Schematic of the control schemas proposed in [45] for different manipulator's spaces where x^* is the desired task space input, q^* is the desired joint space input, q_c is the joint space control variable, u^* is the actuation space variable, u and x are the actuation and task space real variable, q^o is the joint space modelled variable; (C) Schematic of [30] control schema with feed-forward and feedback control where x_{v^*} is the feed-forward task space variable, q_v is the differential joint space variable.*

Entering a more complex modelling approach, VC static modelling based on CR theory is used in [35],[36] and [66]. The first proposed a feedback PID control applied to the first prototype of the MC system described in Section 2.2; the second presented a kinematic control of continuum manipulators with a feed-forward control algorithm that solves the redundant inverse kinematic problem at the velocity level plus a feedback PID control. The last one instead, proposed an inner-outer control strategy. This allows for the tracking of a desired trajectory in the task space (outer-loop) while ensuring that the shape of the manipulator is appropriately regulated (inner-loop PD controller). Even though the CR model includes soft robot non-linearities, one limitation is that CR is still a simplified mathematical model, so the proposed approaches require accurate measurement of the curvature of the manipulator, which may be challenging in some real-world applications.

Among these closed-loop control methods, it can be seen that PID controller is a popular choice. Their popularity is due to good balance between simplicity of its implementation, versatility to control a wide range of systems, and performance since they can be designed to have good stability and robustness. However the latter characteristics can be guaranteed only with an optimal PID parameters' tuning, which be difficult for non-linear systems with time-varying behaviours, thus requiring a deep understanding of the system being controlled [17]. Although there are several methods to tune PID parameters, such as Ziegler-Nichols, Cohen-Coon and optimization methods, most of the time simple manual tuning is performed, especially in complex non-linear systems as continuum robots.

Lastly, in [2] a dynamic CR model is derived and a sliding mode control algorithm is designed to force the system to follow a desired trajectory while simultaneously rejecting disturbances and uncertainties. Although very promising, the sliding mode control suffers from two limitations. First is the controller complexity since it makes the algorithm difficult to tune and implement in real-world applications, especially in cases where real-time control is required. Secondly, the control algorithm relies on accurate knowledge of the system dynamics, and any modeling errors can significantly affect the performance of the control strategy. This can be especially challenging in cases where the continuum robot's parameters or environment are uncertain or difficult to measure.

As an alternative, model-free approaches offer a way to develop more complex and accurate, design-specific models without prior knowledge of the underlying structure or the environment, as well as reducing the computational cost, making them good candidates for real-time applications.

2.3.3.B. Model-Free Control Strategies

One major benefit of model-free approaches is their ability to avoid the need for defining parameters in the configuration or joint space. This means that they can be applied to manipulators of any shape, and complex kinematic models can be developed based on a large amount of sample data. As a result, model-free approaches are particularly useful for highly non-linear, non-uniform, or gravity-influenced systems, as well as those operating in unstructured environments where modelling is difficult [7]. However, when dealing with well-behaved, compact manipulators in known environments, model-based controllers remain more accurate and reliable [28]. Additionally, the black-box nature of model-free approaches makes it difficult to establish stability and convergence proofs [61].

Model-free controllers can be differentiated into two categories (Figure 2.13): Neural Networks (NN) and Reinforcement Learning (RL). These are both powerful techniques for controlling soft and continuum robots, but they have some key differences in how they approach the control problem:

Neural Networks are a type of machine learning model that can learn to map inputs to outputs through a process of training (supervised learning). In the context of soft and continuum robots' control, a neural network might be used for learning a mapping from sensor measurements to motor commands. The network is trained on a set of input/output pairs, and once it has learned this mapping, it can be used for making predictions on new input data.

Reinforcement Learning is a type of machine learning (deep learning) that involves an agent learning to interact with an environment in order to maximize some reward signal. In the context of soft and continuum robots' control, reinforcement learning might be used for learning a policy for controlling the robot's movements. The agent takes actions in the environment, and receives feedback in the form of a reward signal that reflects how well it is doing. By adjusting its actions based on the feedback it receives, the agent can learn to perform the task more effectively over time.

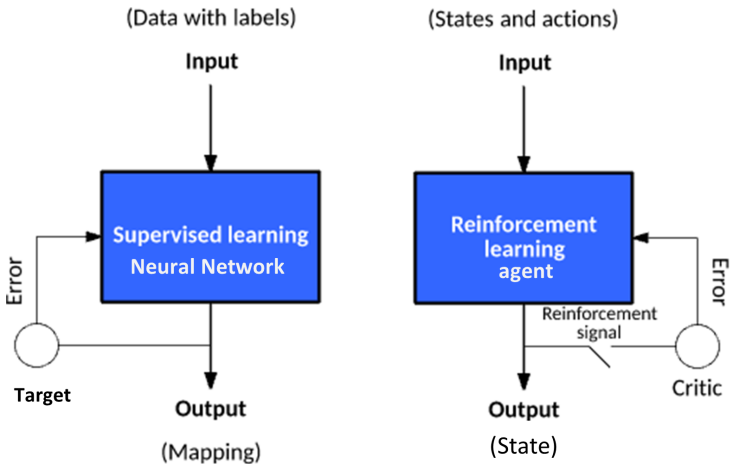

Figure 2.13: *Comparison between Neural Networks and Reinforcement Learning techniques. The former is a type of machine learning whose aim is to learn a mapping between input/output pairs (supervised learning). The latter is a type of deep learning whose aim is to find the optimal policy such that it receives the highest reward from another network (critic) when interacting with the environment.*

The main difference between these two approaches is in how they learn to control the robot. NN are trained on a set of input/output pairs, and once they have learned this mapping, they can be used for controlling the robot in a more deterministic way. So NN are well-suited to problems where there is a clear input/output mapping that can be learned from data. RL, on the other hand, involves the agent actively exploring the environment and learning from feedback, which can make it more flexible and adaptable to changing conditions, making it better suited to problems where there is a complex, dynamic environment that the agent must learn to navigate through trial and error [16]. Both techniques can be effective for controlling soft and continuum robots, and the choice between them will depend on the specific requirements of the task [7, 44].

Although being powerful tools, they do have some limitations that should be considered. They need large amounts of training data, difficulty in generalizing to changing environments or situations, potential for over-fitting, and difficulty in interpreting their internal workings.

Deep Reinforcement Learning (DRL) control strategies for continuum robots are relatively the most recent ones, with the first applications emerging in the past decade. Since then, researchers have explored various DRL-based control approaches for continuum robots due to the unique challenges posed by their high DoFs and non-linear dynamics, which make them difficult to control using traditional control methods. Even though DRL-based control strategies for continuum robots are still in their early stages of development, they

hold great promise, as shown in [63] and [15] in which it was proposed a controller involving the training a RL agent to learn a policy that maps observations of the current state of the system to the optimal control action that should be taken at each time step. The control schema consists of two main components: the RL agent and the soft arm environment. The RL agent is trained using a combination of a deep neural network and a Q-learning algorithm. The neural network takes the current state of the system as input and outputs a Q-value for each possible action. The Q-learning algorithm is used for updating the weights of the neural network based on the reward signal received from the environment. The actions coming from the agent are given to the actuators to control the tension in the soft robot cables, which in turn controls its position in the space. One limitation is that the proposed control schema require a large amount of training data to learn an effective policy. This can be time-consuming and expensive, especially if the soft arm system is complex or has a large number of DoFs.

Going back in time, model-free NN kinematic controllers were first proposed in [27]. In that approach, a Feed-Forward Neural Network (FNN) controller was developed that learned the inverse kinematics of a soft cable-driven manipulator. The FNN controller is trained to predict the cable tensions required to achieve a desired end-effector position and orientation in three-dimensional space. The open-loop controller is designed to operate in real-time and adapt to changes in the manipulator's environment, such as changes in the cable tension or length. The proposed controller was evaluated in simulation and experiments on a physical soft cable-driven manipulator, demonstrating improved tracking performance compared to a traditional inverse kinematics controller. However, it was trained to operate under specific conditions and may not generalize well to new or different environments. In similar approaches, as [52], the training data are obtained experimentally from a physical robot, while in [46] it was proposed a control strategy exploiting a FNN trained using a dataset of pre-recorded catheterization procedures and then used for predicting the motion of the catheter in real-time based on its current position and velocity. The control signals generated by the FNN, which takes as input the current position and velocity readings of the catheter, are the predicted motions of the catheter that are then used for generating the pneumatic actuation signals as output in order to adjust the motion of the catheter in real-time.

At last, in [58], the authors presented a method for learning a closed-loop kinematic controller by integrating the end-effector position as feedback (Figure 2.14). This method is based on a two-step process: first, the system is trained using a dataset of desired end-effector poses and corresponding joint configurations. Once the training is completed, the system is ready to operate in real-time. During operation, the controller receives feedback

from sensors on the manipulator's current state, such as joint angles and position, and uses this information to compute a new joint configuration that will bring the manipulator closer to the desired end-effector pose. In addition, the effectiveness of this control was demonstrated, showing that it is able to accurately track desired end-effector poses and handle unexpected disturbances in unstructured environments.

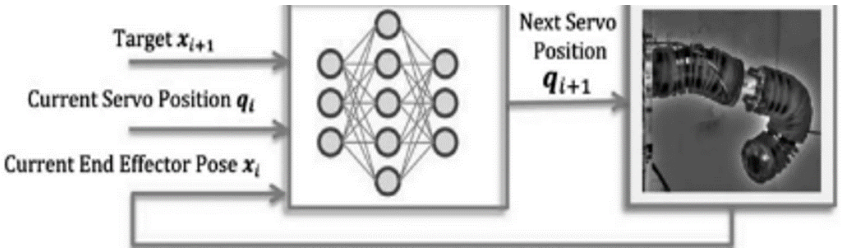

Figure 2.14: *Closed-loop FNN kinematic controller schema from [58]: network inputs are the target at i+1, p_{k+1}, the current servomotors state, q_ik, and the current end-effector pose $\hat{x}_k$. The output is the actuation of the servomotors for the next time instant, q_{i+1}.*

Taking everything into account, the challenging task of controlling a continuum manipulator is now clear. Understanding the kinematics of the robot is essential to controlling it; however, modelling the robot's deformation behaviour, the soft material's non-linear properties and the unstructured environment's uncertainties is extremely difficult. On the other hand, machine learning control methods can offer several advantages over traditional control methods, as they can handle complex, non-linear systems and learn from data that may be difficult to model. Moreover, they have the ability to learn from data and adapt to changing environments, which can improve control performance in dynamic and uncertain systems. Indeed, this last solution seems the most promising to implement in a new MC system control in order to progress from a model-based approach used in [35] to a model-free one, overcoming its previous limitations.

2.4. Aim of the Thesis

With the interest of going a step further in the progress of the ARTERY project, this thesis aims at improving the design of the state-of-the-art MC system prototype and developing a new controller algorithm exploiting a model-free approach. In particular, for the first goal, the limitation described in Section 2.2 will be overcome by introducing:

- A new support architecture in order to meet the clinical requirement of 20° system inclination;
- The Device Handle insertion actuation;

- A new Steerable Guide Handle support to allow its rotation, increasing the DoFs of the MC system.

As regarding the second goal, a new control algorithm will be developed. In particular, a model-free Neural Network Inverse Controller (IKC) following the idea presented in [58] will be implemented applied to the new MC design. Afterwards, the new system and controller will be tested on a real set-up, exploiting Arduino Uno board and ROS communication, in order to determine whether the new prototype is able to reach a desired pose with clinically accepted accuracy of around 2 mm of position error and below 10° of orientation. It is important to mention that this thesis is limited in the intra-cardiac part of the intervention, i.e. shortly after the trans-septal puncture, with the intention of positioning the clip upon the mitral valve.

3 | Materials and Methods

In the following chapter, materials and methods used for designing a new MC system architecture will be presented to overcome physical limitations present in its first prototype. Then, the model-free, closed-loop control algorithm developed for controlling the Delivery Catheter's tip pose will be described.

3.1. Prototype Design

As described in Section 2.3.2, the actions performed on the proximal side of tendon-robots have an effect on its distal end. Thus, for the MC system, rotating ML, AP knobs/motors and inserting the Delivery Catheter inside the Guide Catheter have a result on the distal side of the system (Figure 3.1).

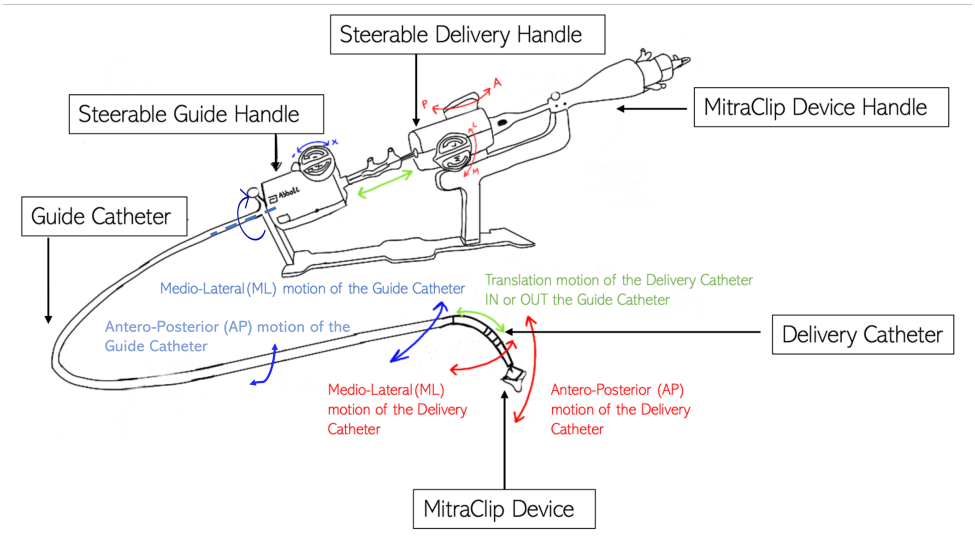

Figure 3.1: *Overview of the MitraClip™ system with possible related actions: acting on the Steerable Guide Handle, the ML and AP bending of the Guide catheter are obtained (blue arrows). Actuating the knobs on the Steerable Delivery Handle, the Delivery Catheter is forced to move in the ML and AP plane (red arrows). The translation movement is obtained by approaching the Steerable Delivery Handle to the Steerable Guide Handle (green line). Adapted from [35].*

Since the first part of this thesis aims at improving the state-of-the-art actuation of the first MC prototype, some key clinical features that are missing in its design are added:

1. System inclination of 20° traditionally achieved by the Stabilizer ;
2. Device Handle mechanism to control tip insertion;
3. Steerable Guide Handle rotation.

SolidWorks® environment was chosen to design this new MC system due to its efficiency in designing and simulating 3D mechanical parts.

3.1.1. Inclined Support Design

The first component to design is the one that guarantees the clinical requirement of MC system inclination of 20°. This support has to host and stabilize the linear motor used for Delivery Catheter insertion, but it also must have enough strength to support the Delivery Catheter Handle that has to be mounted on the motor (Figure 3.2).

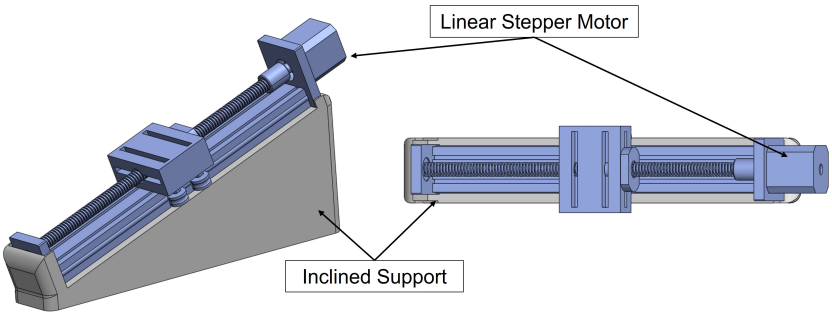

Figure 3.2: *Global and top view of the inclined linear motor support.*

3.1.2. MitraClip™ Device Handle's Actuation Design

As described in Section 2.1, once the MC device is positioned on the correct target, above the mitral valve, it has to be inserted and manoeuvred such that valvular leaflets can be easily grasped by the implant. The previous prototype of the robotic MC system doesn't have any of these motions. Hence, a new independent actuator to add the MC Device insertion is needed and its relative support is designed. First, another inclined support as the one of the previous Section 3.1.1 is exploited to have two parallel independent linear motions, one for the Steerable Delivery Catheter and one for the Device Handle. Then, a structure that guarantees support for the Device Handle and connects it to the linear motor is designed. In addition, a slider to keep the insertion bounded in a straight line is also developed. This completed structure is shown in Figure 3.3.

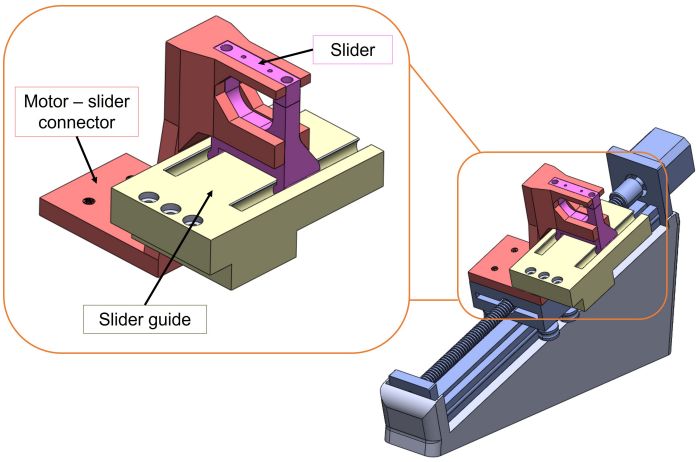

Figure 3.3: *Device Handle's actuation support. On the left: particular of the Device Handle's support that includes (i) motor-slider connector; (ii) a slider ; (iii) slider guide. On the right: Device Handle's support connected to the inclined linear motor.*

Subsequently, this component is added to the first prototyped Steerable Delivery Handle. In this structure there is presence of two supports for the two motors that manage 2 DoF, i.e. rotation in the ML plane and rotation in the AP plane of the Delivery Catheter. To make the support flexible to motor's choice, their position can be adjusted due to the presence of adjustable housing for the screws that connects their supports with the base. The motors are then connected to them by means of metal screws, which guarantee stability. The base of this new structure should be connected to the carriage of the new inclined linear actuator in order insert the Delivery Catheter inside the Guide. This assembly can be seen in Figure 3.4

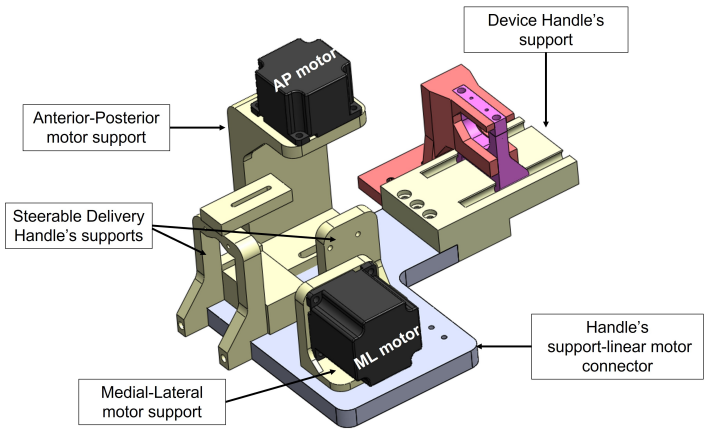

Figure 3.4: *Delivery Handle's complete support comprising: Device Handle support previously described; ML and AP motor's support; Steerable Delivery Handle supports; a base (grey) to connect every component to linear motor actuator.*

3.1.3. Steerable Guide Handle's Actuation Design

By designing properly a Steerable Guide Handle's support, it is possible to have and additional DoF for the MC system which is the rotation of the Guide Catheter on the Anterior-Posterior plane (Figure 3.1). In order to automatize this motion, an additional stepper motor is added whose torque is transmitted to the Steerable Guide Handle through the use of spur gears. Spur gears are a type of mechanical gear that have teeth that run parallel to the axis of rotation and are useful to transmit power and motion between two parallel shafts. The teeth on a spur gear are evenly spaced and have a flat profile, which means that the contact between the teeth is constant as they rotate, resulting in a smooth transfer of power. They can also be used for changing the speed and torque of a rotating system by adjusting the size and number of teeth on the gears (Figure 3.5).

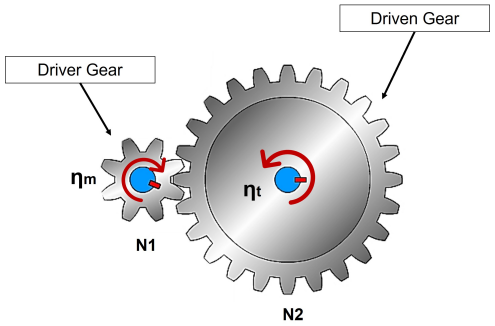

Figure 3.5: *Driver and driven spur gears. The generated torque is function of the driver torque, gears' transmission coefficient* $\frac{N_2}{N_1}$ *and efficiency* $\frac{\eta_t}{\eta_m}$ *as expressed in Equation 3.1.*

For the new MC system, spur gears are designed such that they have enough torque to rotate the Steerable Guide Handle and therefore the Guide Catheter. The transmitted torque can be computed as:

$$T_2 = T_1 \cdot \frac{N_2}{N_1} \cdot \frac{\eta_t}{\eta_m} \tag{3.1}$$

where:

T_2 is the torque generated by the driven gear (in Newton-meters)

T_1 is the torque generated by the driver gear (in Newton-meters)

N_1 is the number of teeth on the driver gear

N_2 is the number of teeth on the driven gear

η_t is the gears' transmission efficiency

η_t is the motor's transmission efficiency

The torque generated by the driving gear T_1 is transferred to the driven gear. The gears' transmission coefficient is given by the ratio of the number of teeth on the driven gear N_2 to the number of teeth on the driving gear N_1 (Equation 3.1). The resulting torque also depends on the efficiency of the motor and gears' transmission as a consequence of energy loss due to friction and heat. The resulting architecture is represented in Figure 3.6.

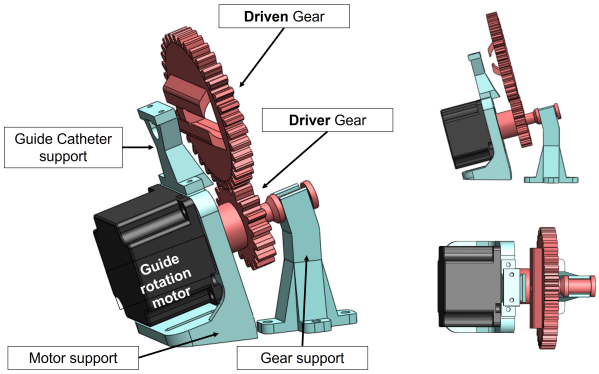

Figure 3.6: *The new Steerable Guide Handle rotation is achieved through spur gear transmission. The designed driver and driven gears possess respectively 18 and 36 teeth, thus making the transmission coefficient equal to 2. Additional components are: a gear support; a catheter support to hold the Guide Catheter in place; an inclined motor's support that follows system inclination of 20°.*

To complete the design of the Steerable Guide Handle, a new support is derived such that it guarantees stability to the handle while also being light and slender. Thus, the total Guide Catheter actuation system is represented in Figure 3.7.

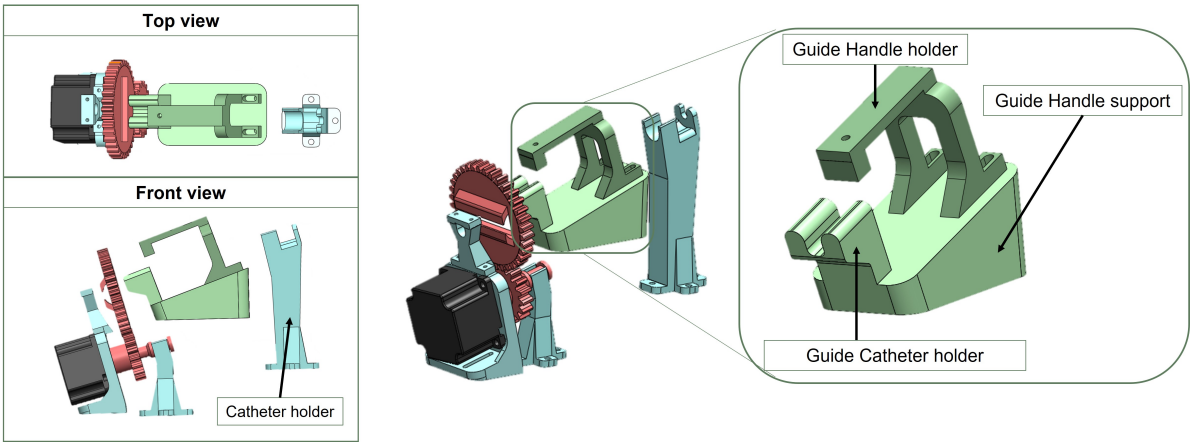

Figure 3.7: *Complete Steerable Guide Catheter actuation system. On the left: top and front views of the actuation and support system comprising motor housing, spur gears, Giode Handle and catheter holder. On the right: particulars of the Guide Handle support.*

Finally, in Figure 3.8, the entire redesigned system is shown, along with a comparison to its old prototype.

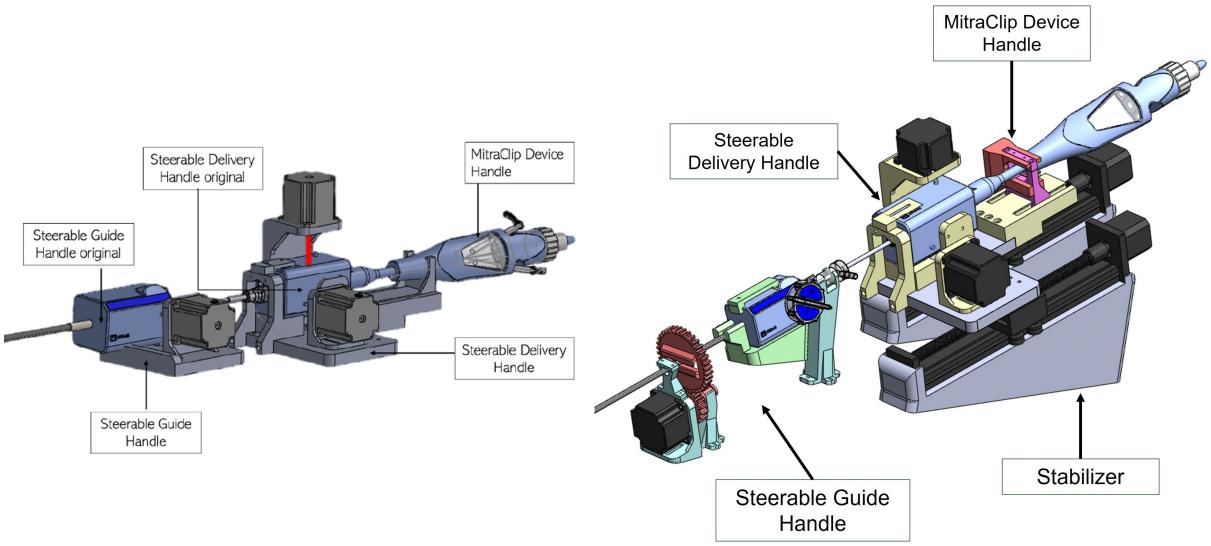

Figure 3.8: *First MitraClip™ robotic system's prototype (left) in comparison to the new proposed mechanical support and actuation (right). The original MitraClip™ components are labelled for both versions.*

3.1.4. Prototype Realization

All the components described in Sections 3.1.1 - 3.1.3 are designed in SolidWorks® environment and printed using the Ultimaker s3 3D printer. Following the same idea described in [35], Acrylonitrile Butadiene Styrene (ABS) material is chosen for printing the support structures, then the actuators are properly fixed by means of metallic screws and Oldham adapters between motors' shaft and original MC actuators (Fig. 3.9).

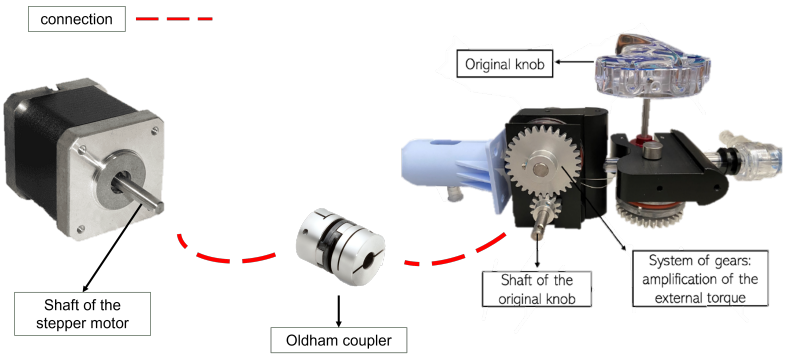

Figure 3.9: *Electrical and MC actuators coupling. From left: electrical motor; Oldham coupler; original MC actuator. Motor's shaft and MC's original shaft are connected through Oldham coupler.*

As regards the electrical components, two Nema 23 Stepper motors (JoyNano) are chosen to pull the tendons, allowing for ML and AP bending with declared control precision of 1.8°±0.09° for each step and maximum holding torque of 2.4 Nm and 1.26 Nm respectively. For the Guide Handle rotation, an additional Nema 23 Stepper motor with a holding torque of 1.26 Nm is used such that the generated torque from the spur gears' transmission (as described in Equation 3.1) is sufficient for the actuation. Then, two Nema 17 Bipolar Stepper Motor (Sainsmart) linear actuators are selected, one connected to a 300 mm linear guide for the insertion of the Delivery Catheter inside the Steerable Guide and the other to a 100 mm linear guide for the insertion of the MC Device. This kind of actuators are chosen for their great precision (±0,03 mm) and their ability to carry a structure with a maximum axial load of 10 kg. Each motor is controlled by a DM556 driver (Jadeshay), with eight current levels and a resolution of 0.5 A. Concerning the micro-controller, the Arduino Uno board is employed, which serves as the central hub for all the electrical components to obtain the control signal from a single device. Lastly, a power supply of 24 V is used.

Figure 3.10 shows the real, 3D-printed system with the chosen electrical components.

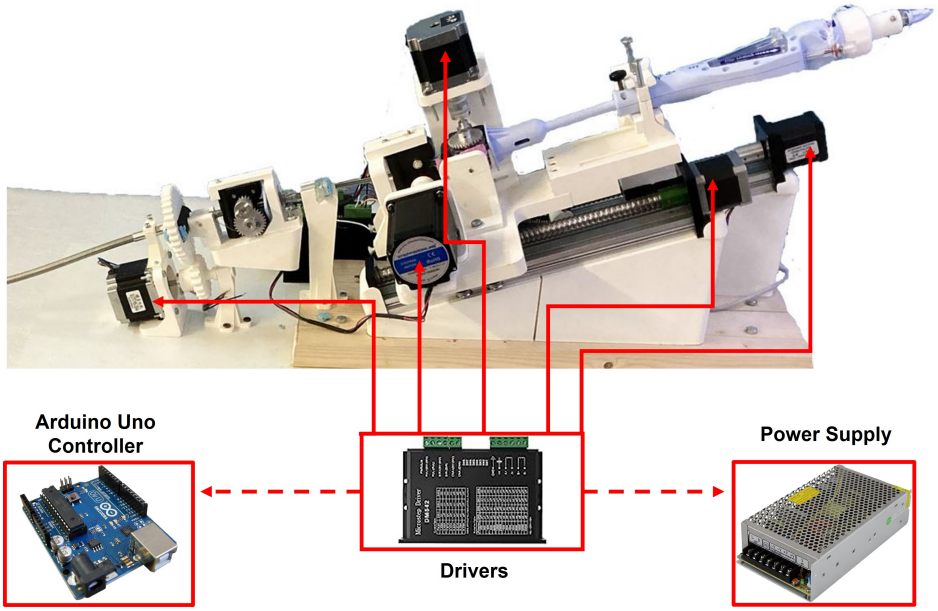

Figure 3.10: *Global 3D printed MC robotic system with its electrical components: the white parts are the 3D printed ABS supports, the Arduino Uno board is employed to actuate the motors, each controlled by drivers and connected to a 24V power supply.*

3.2. Control Algorithm

In this thesis, the control aims at driving MC system actuators in order to bring the Delivery Catheter's tip position and orientation as close as possible to a desired one in 3D space. These poses corresponds to the optimal path's points generated by the Path Planner once the surgeon selects the targeted point of intervention for mitral valve repair.

3.2.1. Closed-loop, Model-free Controller

As stated in Section 2.3.3.A, due to the non-linear nature of this tendon-driven robot, modelling its kinematics analytically becomes difficult and inaccurate since simplifying assumptions are needed. Moreover, points that describe the continuum robot configuration cannot be easily measured, thus approximations are used, introducing additional errors. In addition, external non-ideal factors such as friction, gravity and tendons' slack are excluded in simplified models as the PRB, CC and PCC while they are only estimated in CR modelling.

In contrast to traditional control methods, in Section 2.3.3.B model-free control techniques are explored. Recent works proved that model-free control strategies can provide benefits due to their capability to manage intricate and non-linear systems. Additionally, they have the capacity to acquire knowledge from data and adjust to uncertain environments, leading to enhanced control effectiveness in unpredictable and dynamic systems. Among model-free techniques, Neural-Networks (NN) and Reinforcement Learning (RL) are the most used ones in controlling soft/continuum robots in such conditions. Despite being more recent and highly promising, RL techniques are difficult to implement since they require an active exploration of the environment, navigating through it by trial and errors and learning from feedbacks. Indeed, for RL algorithms it is necessary to find a trade-off between exploring new actions to learn more about the environment and exploiting actions that have been learned to maximize the reward. In addition, the effectiveness of RL depends heavily on the reward signal used for guiding the learning process, especially for complex and multiple tasks where it may be difficult to define a clear objective [21].

Therefore, the proposed control method is a model-free feedback data-driven controller that exploits Multi-Layer Perceptron (MLP) Neural Network capability to fit any non-linear mapping function under the condition of using hidden layers with non-linear activation functions.

3.2.2. Data Generation and Network Training

To control the MC system with a model-free approach, first the mapping between tip poses and actuators state should be established. In order to acquire all feasible Delivery Catheter tip poses without exceeding the physical limitations of finite tendon's length, some preliminary analysis on the maximum number of steps that the motors can perform are done. Then, the number of steps are discretized such that the actuation produces a visible variation of the catheter's distal tip. As regarding the linear insertion, not all the 300 mm of the linear guide lengths are explored, but the limit is chosen to respect two conditions: the first one is to not exceed anatomical atrial boundaries; the second one follows clinical requirement of inserting the Delivery Catheter at a maximum length that corresponds to a second metal ring embedded on the catheter as it is shown in Figure 3.11.

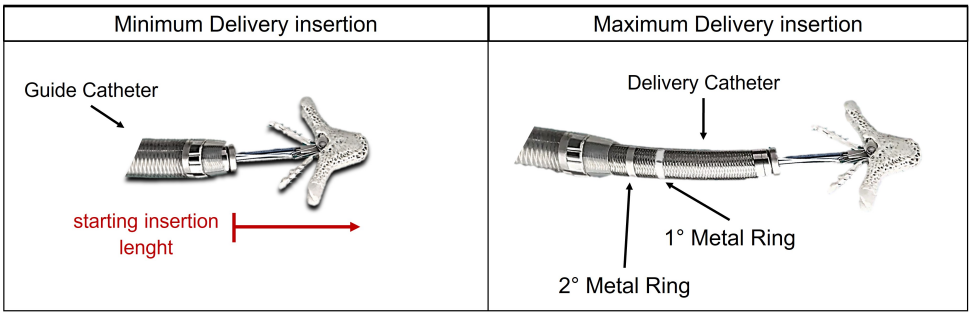

Figure 3.11: *Minimum and maximum Delivery Catheter insertion lengths: the minimum corresponds to catheter's length that makes only the clip implant coming out of the Guide Catheter; the maximum length corresponds to the second metal ring coming out from the Guide Catheter.*

It is important to note that, for this thesis, the motors used for data collection are three: two motors attached to the Delivery Catheter's tendons that enable catheter's motions into ML an AP planes; one linear actuator that enables Delivery Catheter's insertion inside the Guide. The Guide rotation motor introduced previously in the new MC design remains inactivated. This choice is done to make it possible to compare the novel model-free controller performances with the model-based one of the previous MC robotic system by keeping the same number of DoFs.

Once the limits are established, actuation and data acquisition are presented. Data samples used for learning such mapping are generated from the real soft robot set-up by

making it explore its whole workspace. The tip pose corresponding to a particular set of motor commands is registered by using an Electromagnetic (EM) tracking system (NDI Aurora®) which enables real-time tracking of microsensors [10]. To deliver real-time instrument tracking, the EM tracking system is composed of the following four components (Figure 3.12):

1. System Control Unit (SCU);
2. Sensor Interface Unit (SIU);
3. Field Generator (FG);
4. Sensor/s.

The SCU manages the field generator, gathers data from the SIUs, computes the position and orientation of each sensor, and communicates with the host computer through a Type-B USB connection. The SIU strengthens and digitizes the signals produced by the sensors. A maximum of two SIUs can be linked to one SCU. The SIU port can accommodate both 6-DoFs sensor/tools and 5-DoFs sensors/tools. The FG produces a weak, variable EM field that determines the location of the measurement volume. Finally, the sensors operate as reference points within the measurement volume, with position and orientation information transmitted to the host interface for visualization.

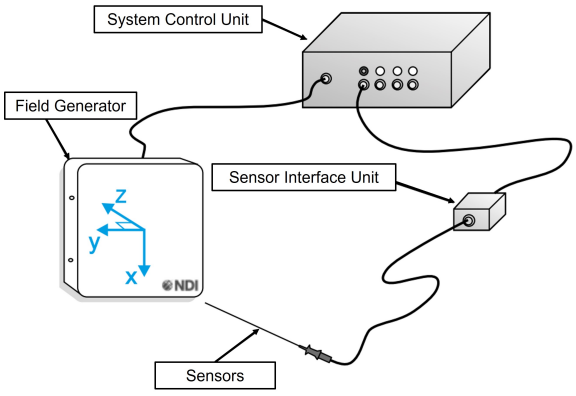

Figure 3.12: *Simplified representation of the EM tracking system (Aurora® NDI) components with its corresponding spatial system axis. Image adapted from [10].*

In order to gather reliable data, a set of three 6 DoF microsensors (RMSPE 0.7 - 1.4 mm) are used, one attached to the catheter's tip (MC clip implant), one attached to the distal end of the Guide Catheter and the last one attached to a fixed location of the set-up. By referring the tip pose with respect to the Guide Catheter pose and calibrating both to a

fixed point instead of the global EM reference system, we can minimize errors caused by the FG motion. This sensors' configuration can be seen in Figure 3.13.

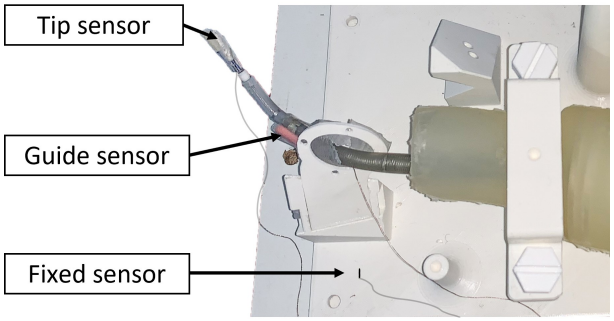

Figure 3.13: *Sensors configuration for data acquisition. Three 6-DoF EM microsensors are used, one attached to the catheter's tip, one attached to the distal end of the Guide Catheter and the last one attached to a fixed location of the set-up.*

Since the soft robot is composed of flexible materials, once the motors are actuated, a residual motion can be observed. In order to reduce this viscous effect and also minimize sensors' uncertainties, for each actuation, the relative tip pose is registered for 2 seconds at 4 Hz, then discarding the first 4 samples, and averaging the last 4 ones. The mapping of the whole workspace is covered by a total of 9808 points, further processed and reduced to discard all tip poses where tendons show backlash behaviour (no motion produced after actuation). This is due to the lack of tendon tension that occurs when motors change their rotation direction. Since the data are derived from the real set-up, they could effectively reduce the error caused by mathematical model that neglects those non-linear factors. All the gathered data are pictured inside the real set-up as shown in Figure 3.14

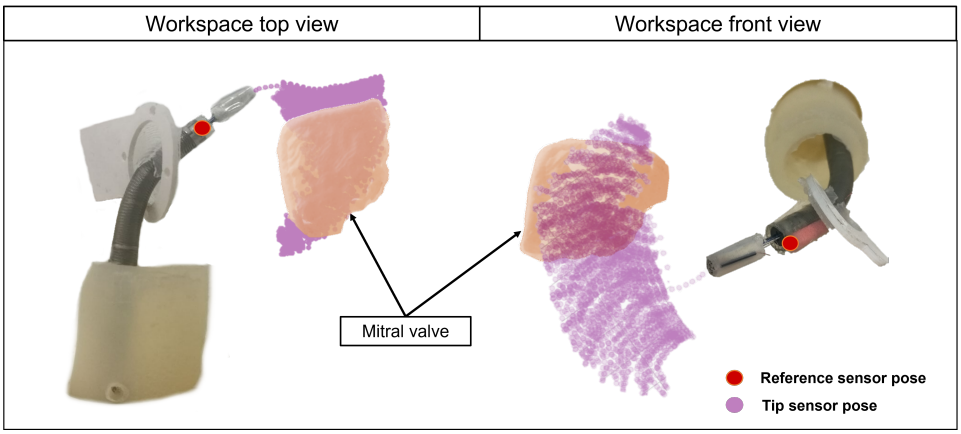

Figure 3.14: *Dataset visualization inside the real set-up. Tip poses (pink dots) and Guide Catheterd poses (red dot) are registered through two EM 6-DoF microsensors, then a transformation to refer tip poses to Guide poses is applied.*

Once the complete data-set of motor actuation and poses is obtained, MLP model supervised training can be performed. The designed controller network has an input layer with 17 neurons. The network inputs are:

- **Current tip pose** expressed in 3D Cartesian coordinates for position and quaternion for orientation;
- **Actuators state** corresponding to current tip pose;
- **Target tip pose** also expressed with 3D Cartesian coordinates and quaternion.

The output layer has 3 neurons: the outputs produced from this network are the predicted number of motor steps needed to pass from current pose to the desired tip pose. Each of the tree outputs is related to one of the three controlled motors stated previously (Delivery Catheter linear actuator, ML and AP bending motors).

The optimal set of network hyperparameters (number of hidden layers, number of hidden neurons, learning rate, activation function, etc.) are found through the Python Keras Tuner library. With this library, given a set of hyperparameters, it is possible to find the best combination that optimizes a specified objective function. For this mapping, the set of hyperparameters used for the search are summarized in Table 3.1, exploring between 1000 combinations using Adam optimizer and Mean Absolute Error minimization as objective function.

	Hidden Layers	Hidden Neurons	Learning Rate	Activation
value	1 - 4	16 - 64	0.01 - 0.0001	tanh - sigmoid

Table 3.1: *Network hyperparameters research set. The possible combinations performed by Keras Tuner are between the number of hidden layers that goes from 1 to 4; the number hidden neurons can be selected between 16 to 64 (stepping 4 by 4); learning rate that can assume three possible values among 0.01, 0.001, 0.0001; lastly the non-linear hidden layer activation function can be chosen between hyperbolic tangent and sigmoid.*

The optimal number of hidden layers found with Keras Tuner is 2 with 56 and 60 neurons respectively, with hyperbolic tangent as activation function, and a learning rate of 0.001.

Once the optimal network structure is found, and its training is completed, the evaluation of the developed a Neural Network Inverse Kinematic Controller (IKC) shown in Figure 3.15 can be performed through some experimental protocols that will be described in the following chapter.

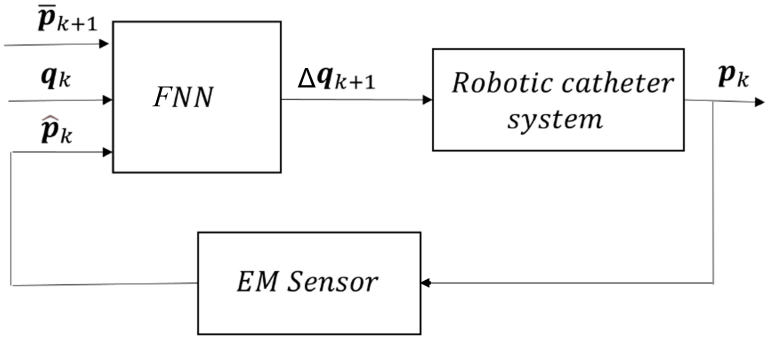

Figure 3.15: *Schema of the proposed Inverse Kinematic Controller. The inputs are the desired pose at k+1, $\bar{p}_{k+1}$, the current stepper motors state, q_k, and the current tip pose $\hat{p}_k$ measured by the EM sensor. The output is the number of stepper motor steps for the next time instant, Δq_{k+1}, in order to reach target pose starting from current pose.*

3.3. Robot Operating System Integration

Before introducing the experimental protocol, it is necessary to integrate different modules of the robotic MC system. The tool that allows this operation is Robot Operating System (ROS). ROS is an open-source framework with a set of software libraries and tools that helps in managing hardware resources and controlling low-level devices, as well as higher-level functionalities such as perception, planning, and control. ROS architecture is based on a distributed system of *nodes*, each running a specific task and communicating with each other using *messages*. For this set-up, the communicating nodes are:

- **Path Points Node:** communicates to IKC Node the sequential target poses p_t computed by the Path Planner Module when a desired point p_d is selected on the mitral valve
- **IKC Node:** takes as input target pose p_t, current tip pose p_r from EM Node and actuators' state from Arduino Node, then computes and communicates the needed actuation $\Delta q_{a,\ a\ =\ 1,2,3}$ to Arduino Node in order to reach target point p_t;
- **EM Tracking System Node:** communicates EM sensors poses p_r to IKC Node;
- **Low Level Control Node:** receives the actuation from IKC Node Δq_a, executes it by controlling the motors then communicates of the new actuators state q_a to IKC Node.

The described communication schema is represented in Figure 3.16.

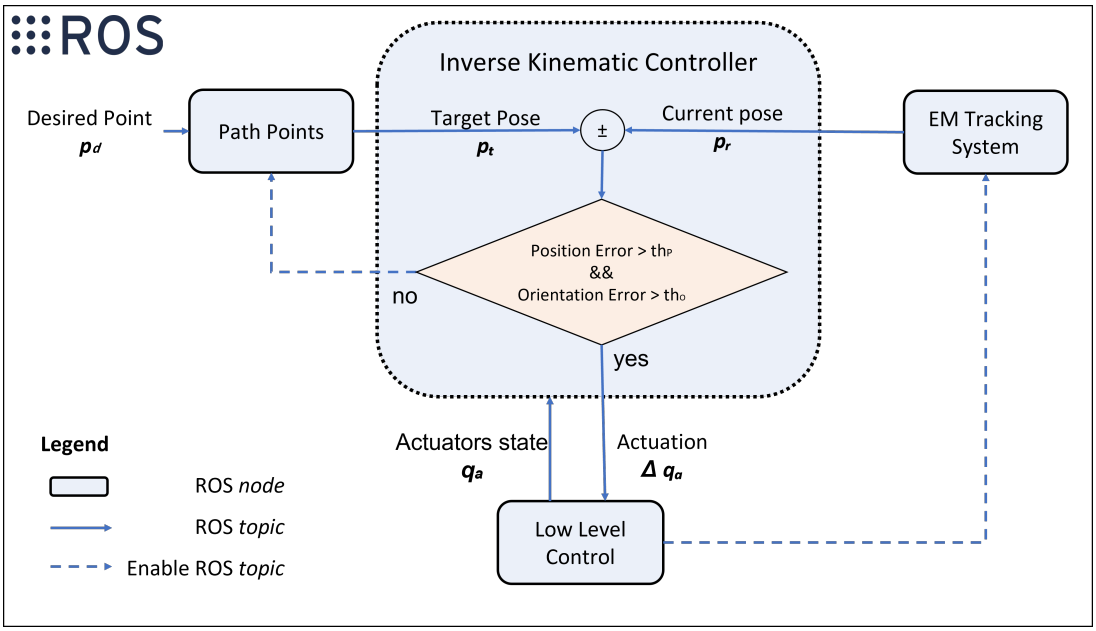

Figure 3.16: *ROS implementation of the control algorithm. The Path Points Node provides sequentially the point of the path computed by the path planner to the IKC Node, which produces the control variable for the system. After the actuation, the EM System reading is enabled: the comparison between the target pose and the real one is performed and if the error is bigger than the threshold of 2 mm of euclidean distance or 10° of orientation for yaw, pitch and roll angles, the new actuation is computed by IKC Node; conversely, a new point of the path is passed.*

ROS version used for the communication is Noetic and it runs on Ubuntu 20.04.4 LTS.

4 | Experimental Method

This chapter will illustrate the real set-up used for testing the controller developed in Section 3.2 and defines the experimental protocols implemented to ensure its functionality and validate its performances.

4.1. Experimental Set-up

To test the controller, the physical set-up comprehends the following components:

- The new MC robotic system re-designed as described in Section 3.1.4;
- Two computers connected to the same network, one used by IKC Module (PC1) and the other used for communicating the optimal path computed by Path Planner Module (PC2);
- EM tracking system (Aurora® NDI) for acquiring the position and the orientation of the sensors placed on MC Device;
- A phantom to simulate the anatomical environment of the vessel, in which the catheter is inserted, and some heart components.

All these elements are depicted in Figure 4.1.

In this set-up, the physical phantom of the femoral vein is introduced since the catheter behaves differently in a constrained environment rather than free-space. It consists in a model of femoral and inferior vena cava realized in silicone polymers to emulate the deformability of the vessel. Then, it is stabilized in the correct position through some 3D printed ABS supports. As regarding the heart components, the mitral valve is 3D printed in ABS from an anatomical model of a real CT scan, while the fossa ovalis is realized in silicone polymers and supported with another 3D printed ABS component. The complete anatomical set-up is shown in Figure 4.2.

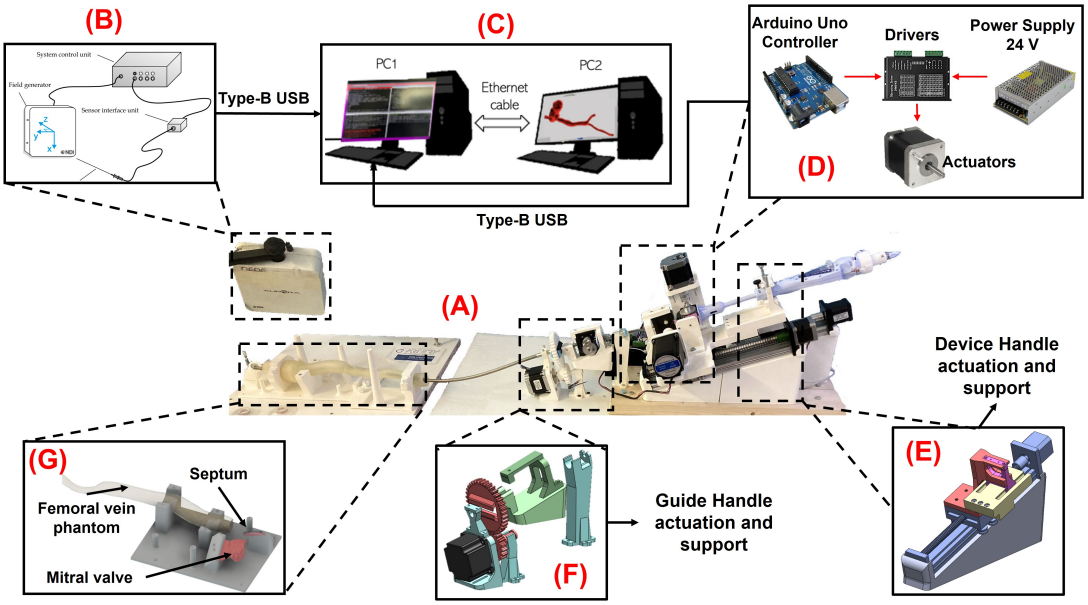

Figure 4.1: *Complete robotic MC system set-up: (A) catheter actuation plant; (B) EM tracking system; (C) PC1 used for running the ROS environment on Ubuntu 20.04.4 LTS and PC2 used for Unity simulation on Windows 10; (D) electrical devices and power source; (E) designed inclined Stabilizer and Device Handle's actuation for clip insertion; (F) design of the motorized Guide Handle's rotation; (G) patient-specific physical phantom and heart components.*

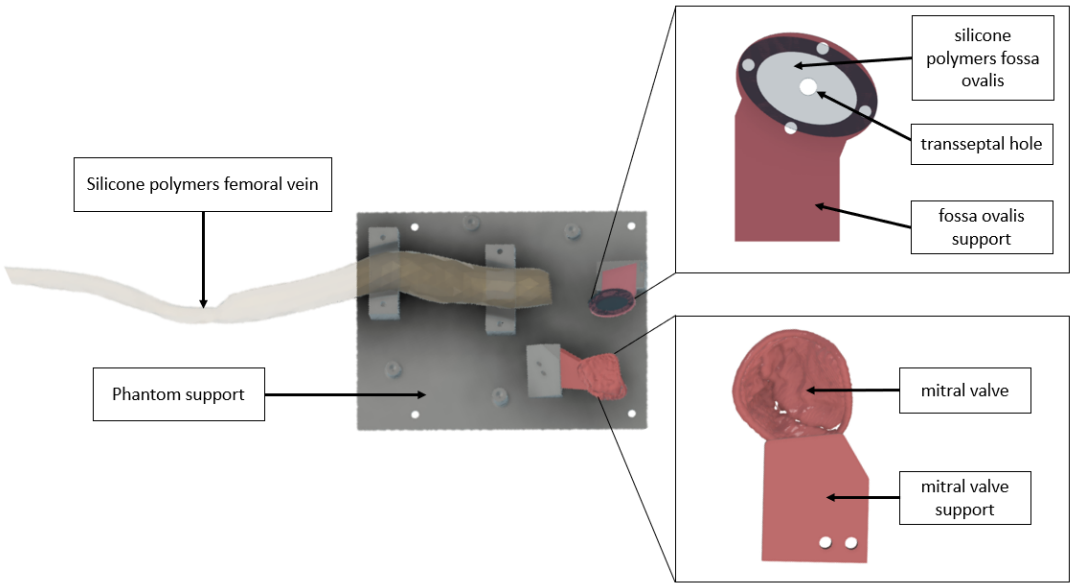

Figure 4.2: *Physical set-up of the anatomical components. On the left: top view of the complete anatomical set-up composed of the femoral vein, its support, the mitral valve and the fossa ovalis. On the right: detailed front view of the fossa ovalis and the mitral valve.*

It is important to note that the Guide and the Delivery Catheters should be inserted manually inside the phantom, until the Guide Catheter is positioned 2 *cm* through the trans-septal hole made in the fossa ovalis. From this point, the intra-cardiac part of the intervention starts and the MC Device is actuated and controlled.

Concerning the computers, PC1 is equipped with ROS environment where a ROS package must be created so that the experimental protocols work. To allow the communication among the modules and the implementation of the control algorithm, the following executable files are inserted in the ROS packages:

- Rosserial to allow serial communication between the Arduino and ROS environment;
- EM tracker system package to perform and visualize real-time tracking;
- Python code that implements IKC algorithm;
- Arduino IDE code to actuate the motors.

On the other hand, PC2 is equipped with Unity's simulation environment used by the Path Planner Module.

The EM system enables unobstructed real-time tracking of EM microsensors, which is a solution perfectly suited for a real-time feedback controller as the one developed in this thesis. For this reason, the experimental protocols include three 6-DoFs EM sensors, one located on the tip of the MC device, one placed at the distal end of the Guide Catheter and the last one is placed to a fixed point of the set-up, in the same way as described in Section 3.2.2 for data generation (Fig. 3.13). This is done to refer the tip to the Guide Catheter with the same transformation that was applied to the data used for training the IKC network, calibrated with respect to the fixed point rather than FG reference system. As a result, the data read from the tip sensor becomes independent from any position of FG in space, therefore it can be moved without changing its reference.

4.2. Experimental Protocols

The experimental protocols described in this section will be used for evaluating the performances of the proposed controller in terms of path tracking accuracy of position and orientation. In particular, two aspects of the MC system control will be evaluated: the first part focuses on the performances comparison of the model-free controller approach with respect to the state-of-the-art model-based one developed in [35]. The second part involves experiments to analyse the performance of the IKC controller in relation to the number of points of the optimal path.

However, before proceeding with the experimental phases, some preliminary tests are performed to have the experiments' statistical relevance of at least 85% confidence by determining:

- Number of paths for test's **variability**;
- Paths repetitions for test's **repeatability**;
- Number of path's points for controller **characterization** with respect to points distance.

With the assumption of normality distribution, this evaluation lead to the selection of 9 different paths, with a repetitions of 4 trials each and a minimum number of 5 path's points.

Taking into consideration this investigation, the following experiments will be performed:

1. Five-points path tracking with the model-based PID controller from [35] applied to the developed MC robotic system (Section 2.2);
2. Five-points path tracking with the model-free IKC developed in Section 3.2;
3. Path tracking with model-free IKC using 10-points, 15-points and 20-points paths.

For the reader's convenience, the aforementioned experiments will be named respectively **PID-5**, **IKC-5**, **IKC-10**, **IKC-15**, **IKC-20**.

4.2.1. Paths Choice

To achieve a clear overview of the controller performances with respect to path and catheter behaviour, some considerations on the clinical aspects of the MC procedure are reported. Since the traditional way of performing the TMVr with the MC system requires a fixed insertion length between two metal rings (as previously described in Fig. 3.11), this constraint is also considered for the path generation of the selected target points. Then, a combination of feasible ML and AP curvatures of the Delivery Catheter are selected. In particular, these curvature are chosen such that the last path point (target) lies in an area on the mitral valve where MR could occur. This area is considered by taking into account the mitral valve commissural diameter, which is a line defined between the two interconnection points of the mitral leaflets (Figure 4.3).

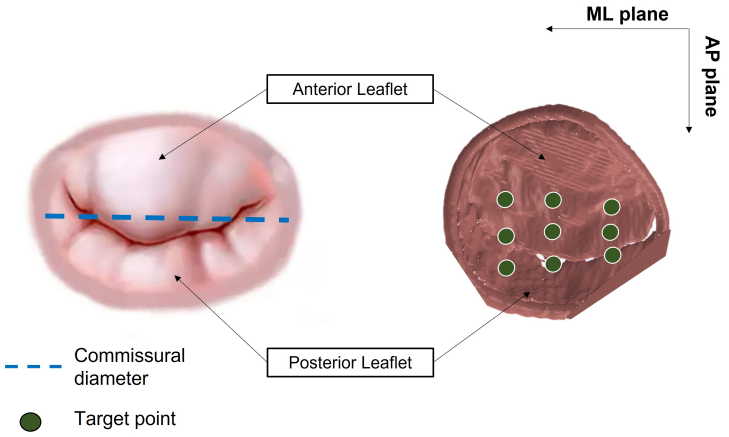

Figure 4.3: *Nine paths' target on the mitral valve lies around the commissural diameter of the valvular leaflets by taking into consideration the combination of three different ML and three AP Delivery Catheter's curvatures and a fixed insertion length.*

Thus, these paths can be characterized by a fixed insertion length and the combination of three different ML and AP curvatures of the Delivery Catheter, with a set of 9 target points placed on the mitral valve regurgitation site.

4.2.2. Controller Evaluation

To validate the proposed MC system controller, position and orientation accuracy are evaluated respectively in terms of Euclidean Distance (ED) and Mean Absolute Error (MAE) between desired pose p_t, and measured pose p_r (Equations 4.1, 4.2). In particular, for orientation the standard yaw, pitch and roll rotation axis are considered.

$$ED = d(p_t, p_r) = \sqrt{\sum_{i=1}^{n} (p_{t_i} - p_{r_i})^2} \tag{4.1}$$

$$MAE = \frac{1}{n} \sum_{i=1}^{n} |p_{t_i} - p_{r_i}| \tag{4.2}$$

where p_{t_i} and p_{r_i} are the i-th elements of vectors p_t and p_r, respectively.

For all the experiments, both model-based and model-free controllers can attempt to reach target path point for five times. The reached position and the reached orientation are collected through EM sensors. The desired pose is considered reached if the ED is below a threshold of 2 mm and orientation MAE is below a threshold of 10° for all angles.

Each of the aforementioned experiments is performed on all 9 paths, repeating the procedure four times. An example of the complete experimental set-up with a five-points path tracking objective is represented in Figure 4.4.

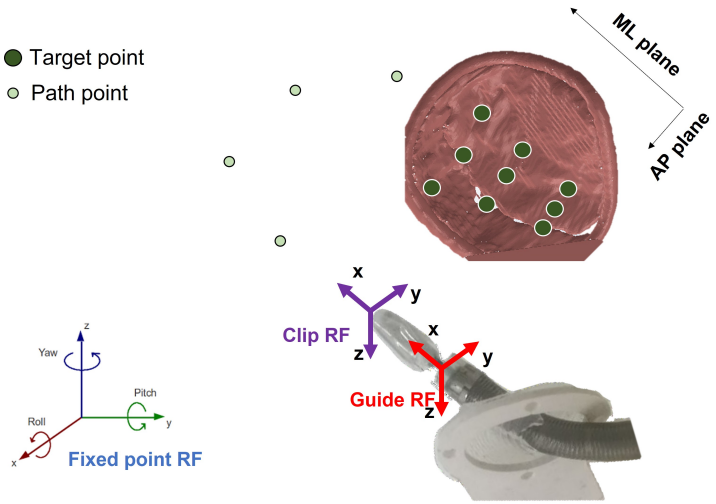

Figure 4.4: *Example of 5-points path tracking experimental set-up, consisting in controlling position and orientation of the clip through all path's points up to the mitral valve target point. Current pose is measured from the EM sensor positioned on the clip referred to the Guide sensor, both expressed with respect to a fixed point in space used for calibration. These sensors are here represented with their Reference Frame (RF).*

5 | Results

In this chapter, the data collected in the experiments will be shown. For completeness, the Appendix A will that covers the analysis of the path's repetitions data, to determine whether they belong to the same distribution (i.e. carry the same information) and if it is normally distributed or not. In the results, the 9 different paths' distribution will be also examinated for the same aforementioned reasons.

5.1. Paths Distribution Comparison

The following investigation focuses on the 9 tested paths' distribution. As previously mentioned, these paths are characterised by different combinations of ML and AP catheter's curvature, identified with letters from *A* to *I*. For all experiments (**IKC-5**, **PID-5**, **IKC-10**, **IKC-15**, **IKC-20**), it is analysed if the paths belong to the same distribution through quantitative and qualitative tests.

5.1.1. IKC-5 Paths Distribution

Euclidean Distance

For this experiment, in Figure 5.1 it is represented all paths distribution from *A* to *I*, which have been analysed and verified to belong to the same non-normal distribution. The measured data can be grouped, averaged and studied as a single one (Figure 5.2 A). However, it is also important to investigate the ED measure for all points, in particular the last one, which corresponds to the target point on the mitral valve (Figure 5.2 B).

ED on target point is normally distributed, thus the error can be characterized by the *mean value* and *standard deviation* of **3.95 ± 0.85 mm**.

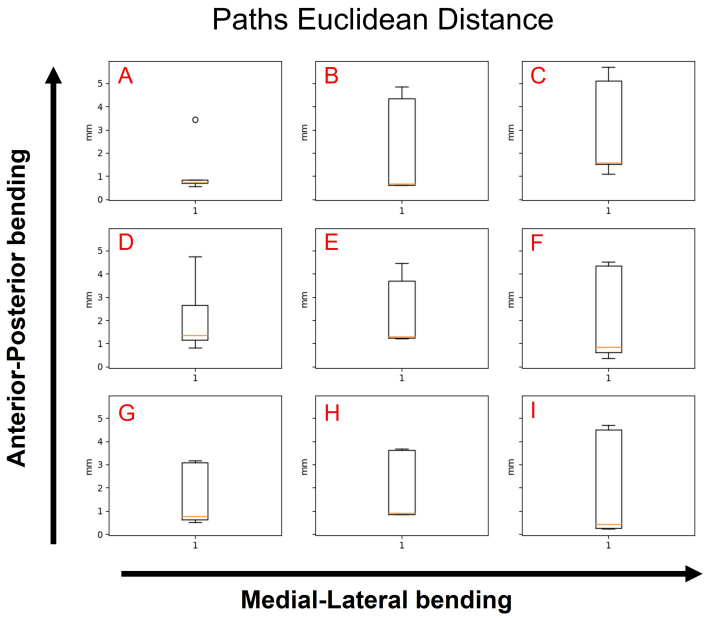

Figure 5.1: *IKC-5 paths distribution. Nine different paths characterised by distinct catheter's ML and AP curvatures (A - I) are investigated. The quantitative analysis of paths distribution is shown through box-plots representation.*

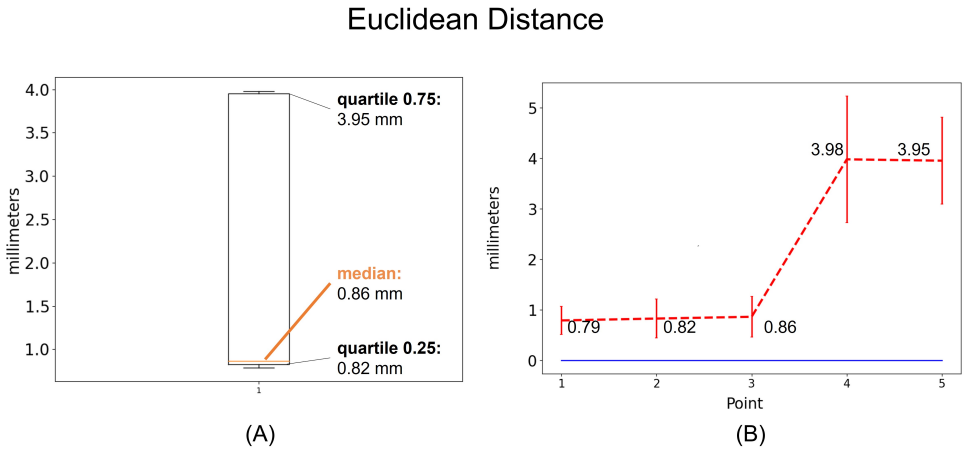

Figure 5.2: *IKC-5 Path Euclidean Distance. (A) represents the euclidean distances of all grouped paths. Since it is non-normally distributed, median and 25% - 75% quartiles are displayed; (B) Path's points euclidean distances displayed with error-bars where the last one represents the target on the mitral valve.*

Orientation Mean Absolute Error

In the same way as the position ED distribution, the yaw, pitch and roll MAE distribution will be examined for this experiment. Figure 5.3-A shows the MAE of all angles in the

different paths (A to I). Since distribution analysis lead to the the conclusion that their distributions are equal, these data are grouped and averaged for each angle, as shown in Figure 5.3-B. In Figure 5.4 it is represented the MAE of each path point, with a particular focus on the mitral valve target point.

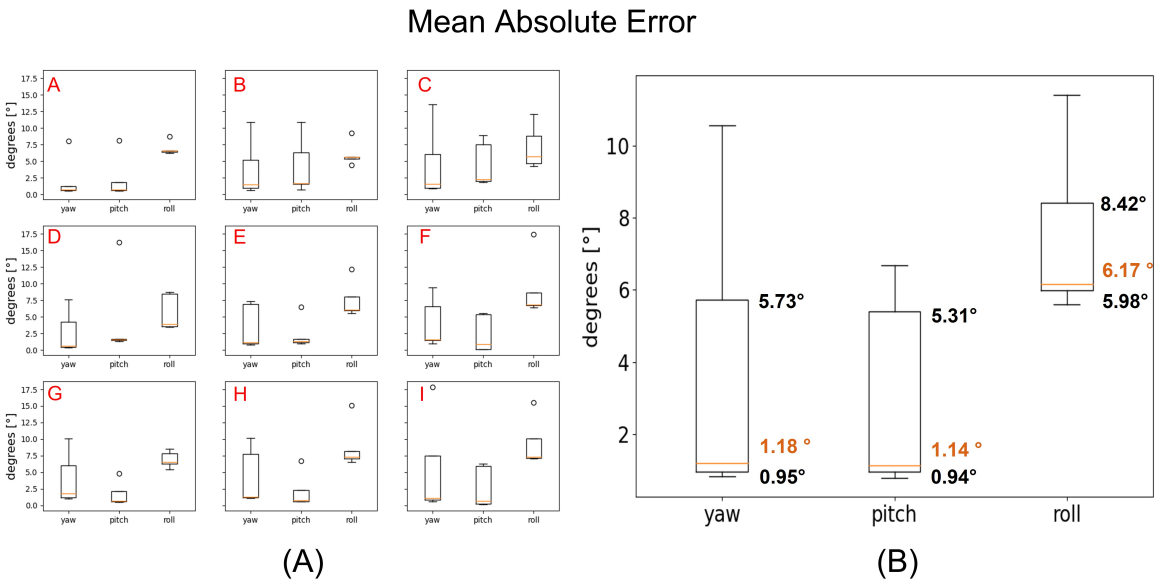

Figure 5.3: *IKC-5 Paths Orientation Mean Absolute Error. Nine different paths characterised by distinct catheter's ML and AP curvatures (A - I) are investigated. On the left: quantitative analysis of the single paths distribution through box-plots. On the right: single box-plot representation of the unified 9 paths angles MAE, with their median and quartiles values.*

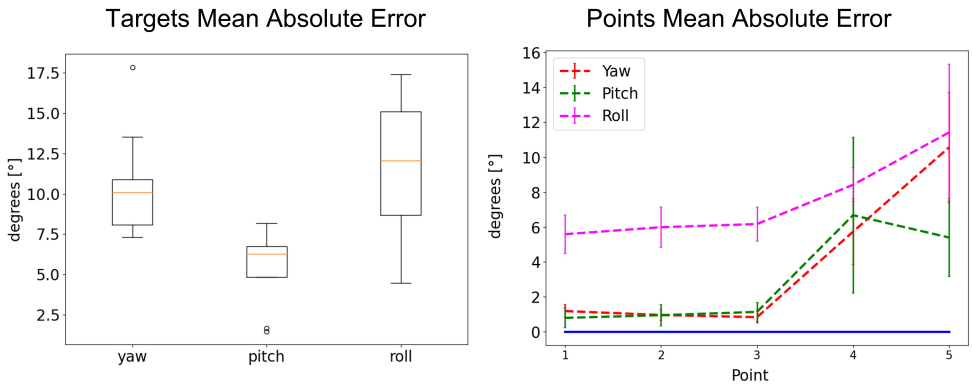

Figure 5.4: *IKC-5 Target Orientation Mean Absolute Error. On the left: yaw, pitch and roll target point MAE. On the right: yaw, pitch and roll angles along path's points represented with error-bars.*

Since yaw, pitch and roll angles MAE are normally distributed, the error can be described

by the error can be described by *mean-value* and *standard deviation*. In particular, for the three angles results:

- Yaw: **10.56 ± 3.14 °**;
- Pitch: **5.39 ± 2.24 °**;
- Roll: **11.42 ± 3.91 °**.

5.1.2. PID-5 Paths Distribution

Euclidean Distance

Also for this experiment, it is demonstrated that all paths belong to the same non-normal distribution represented in Figure 5.5.

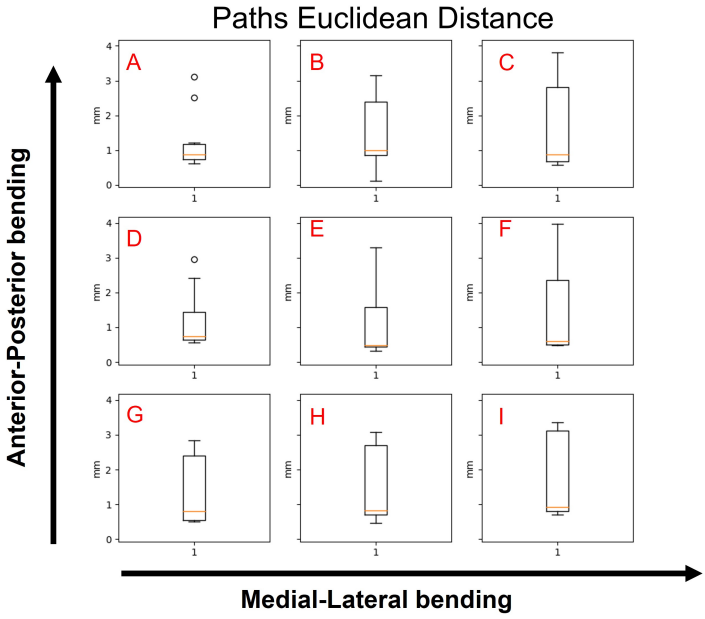

Figure 5.5: *PID-5 paths distribution. Nine different paths characterised by distinct catheter's ML and AP curvatures (A - I) are investigated. The quantitative analysis of paths distribution is shown through box-plots representation.*

The measured data can be grouped, averaged and studied as a single one (Figure 5.6 A), and the ED measure for all path's points is analysed (Figure 5.6 B), focusing on the last target point on the mitral valve.

ED on target point is normally distributed, thus the error is described by *mean-value* and *standard deviation* of **7.54 ± 1.51 mm**.

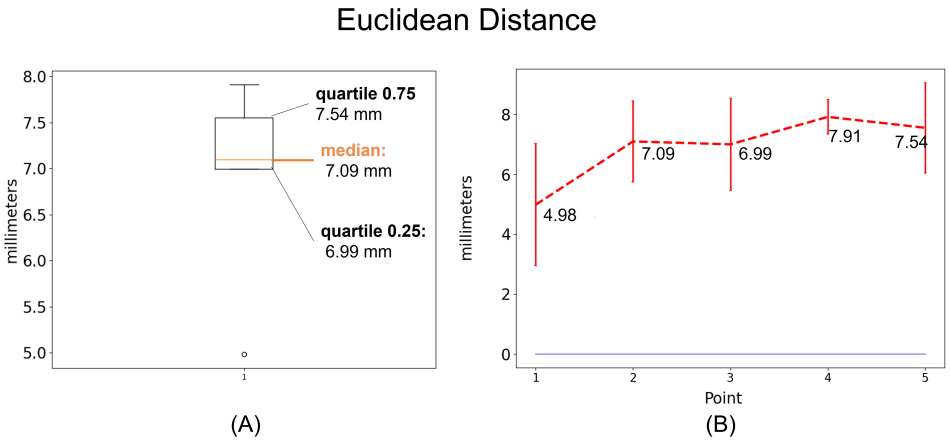

Figure 5.6: *PID-5 Path Euclidean Distance. (A) represents the euclidean distances of all grouped paths. Since it is non-normally distributed, median and 25% - 75% quartiles are displayed; (B) Path's points euclidean distances displayed with error-bars where the last one represents the target on the mitral valve.*

Orientation Mean Absolute Error

Figure 5.7-A shows the MAE of all angles in the different paths (A to I). Since distribution analysis lead to the the conclusion that their distributions are equal, these data are grouped and averaged for each angle, as shown in Figure 5.7-B.

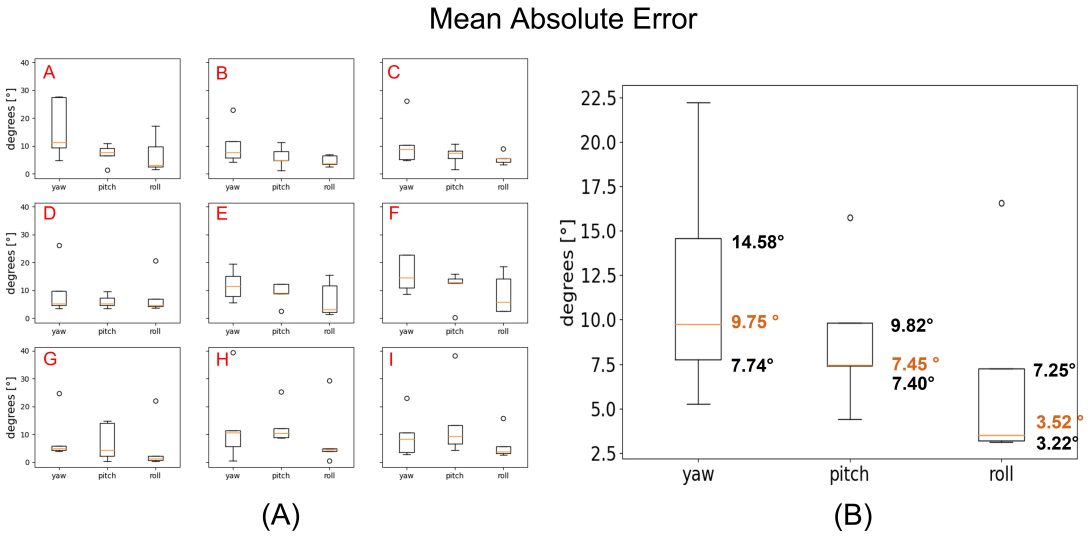

Figure 5.7: *PID-5 Paths Orientation Mean Absolute Error. Nine different paths characterised by distinct catheter's ML and AP curvatures (A - I) are investigated. On the left: quantitative analysis of the single paths distribution through box-plots. On the right: single box-plot representation of the unified 9 paths angles MAE, with their median and quartiles values.*

Orientation errors on path points are examined, with a particular focus on target point as depicted in Figure 5.8.

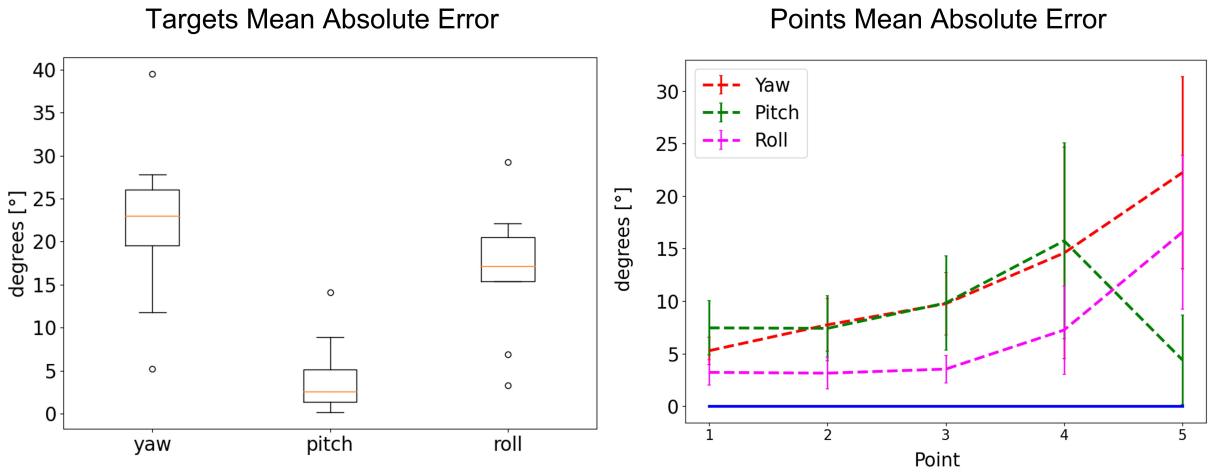

Figure 5.8: *PID-5 Target Orientation Mean Absolute Error. On the left: yaw, pitch and roll angles along path's points. On the right: yaw, pitch and roll target points MAE represented with error-bars.*

Yaw, pitch and roll angles MAE are normally distributed, thus the error can be described by *mean-value* and *standard deviation*. In particular, for the three angles results:

- Yaw: **22.23 ± 9.16 °**;
- Pitch: **4.40 ± 4.25 °**;
- Roll: **16.56 ± 7.33 °**.

5.1.3. IKC-10, IKC-15, IKC-20 Paths Distribution

Euclidean Distance

Lastly, for each of these experiments, it is examined if the 9 paths also follow the same distribution (Figure 5.9). In the same way as before, the ED measures are analysed for the whole experiments datasets (Fig 5.10 A) and for each path point (Figure 5.10 B). The normality assessment allows to characterise the target points results with *mean value* and *standard deviation*. In particular for these experiments they result:

- IKC-10: **3.02 ± 0.52 mm**;
- IKC-15: **2.39 ± 0.12 mm**
- IKC-20: **2.37 ± 0.13 mm**

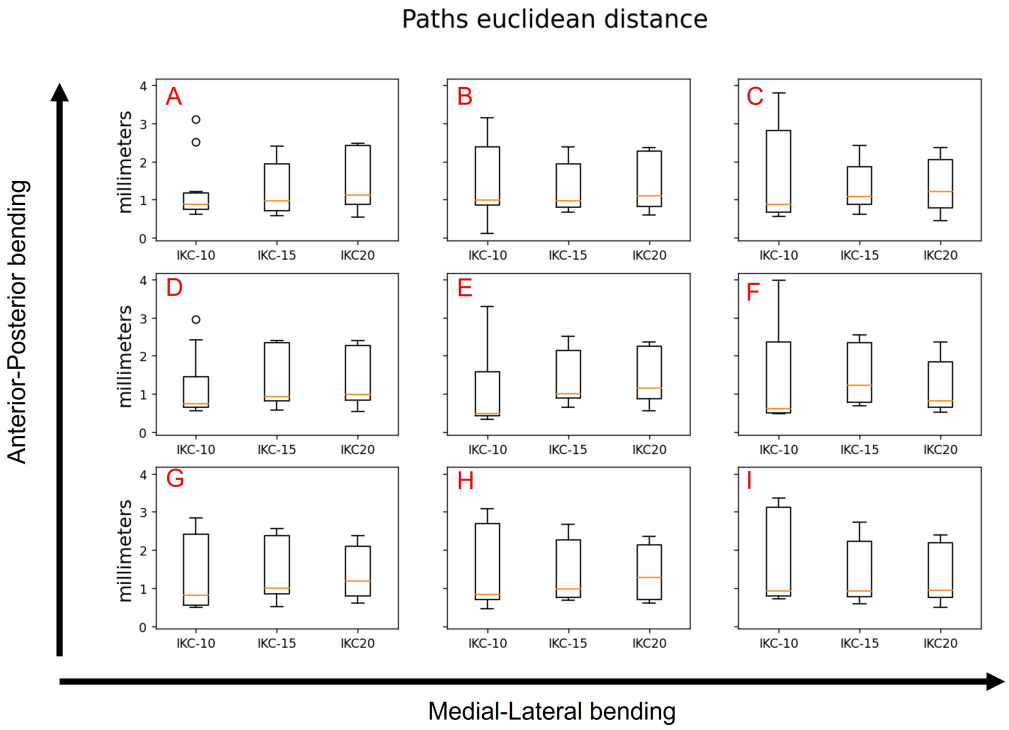

Figure 5.9: *IKC-10, IKC-15, IKC-20 paths distribution. Nine different paths characterised by distinct catheter's ML and AP curvatures (A - I) are investigated. For all three experiments, it is demonstrated that the 9 paths belong to the same non-normal distribution.*

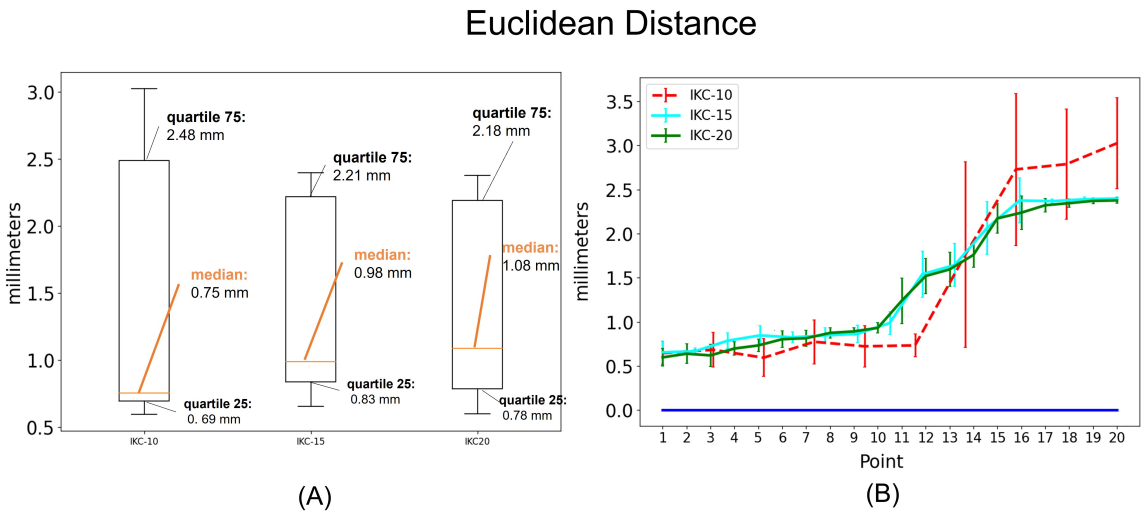

Figure 5.10: *IKC-10, IKC-15, IKC-20 Path Euclidean Distance. (A) represents the euclidean distances of all grouped paths of the three experiments. Since they are non-normally distributed, median and 25% - 75% quartiles are displayed; (B) Path's points euclidean distances represented with error-bars where the last one represents the target point on the mitral valve.*

Orientation Mean Absolute Error

In the experiments, the MAE of yaw, pitch and roll angles for all paths from A to I, is analysed in the same way as previously described. The distribution analysis lead to the the conclusion that their distributions are equal. Then, the analysis on angles MAE on path points is performed, focusing on the target point, as shown in Figure 5.11.

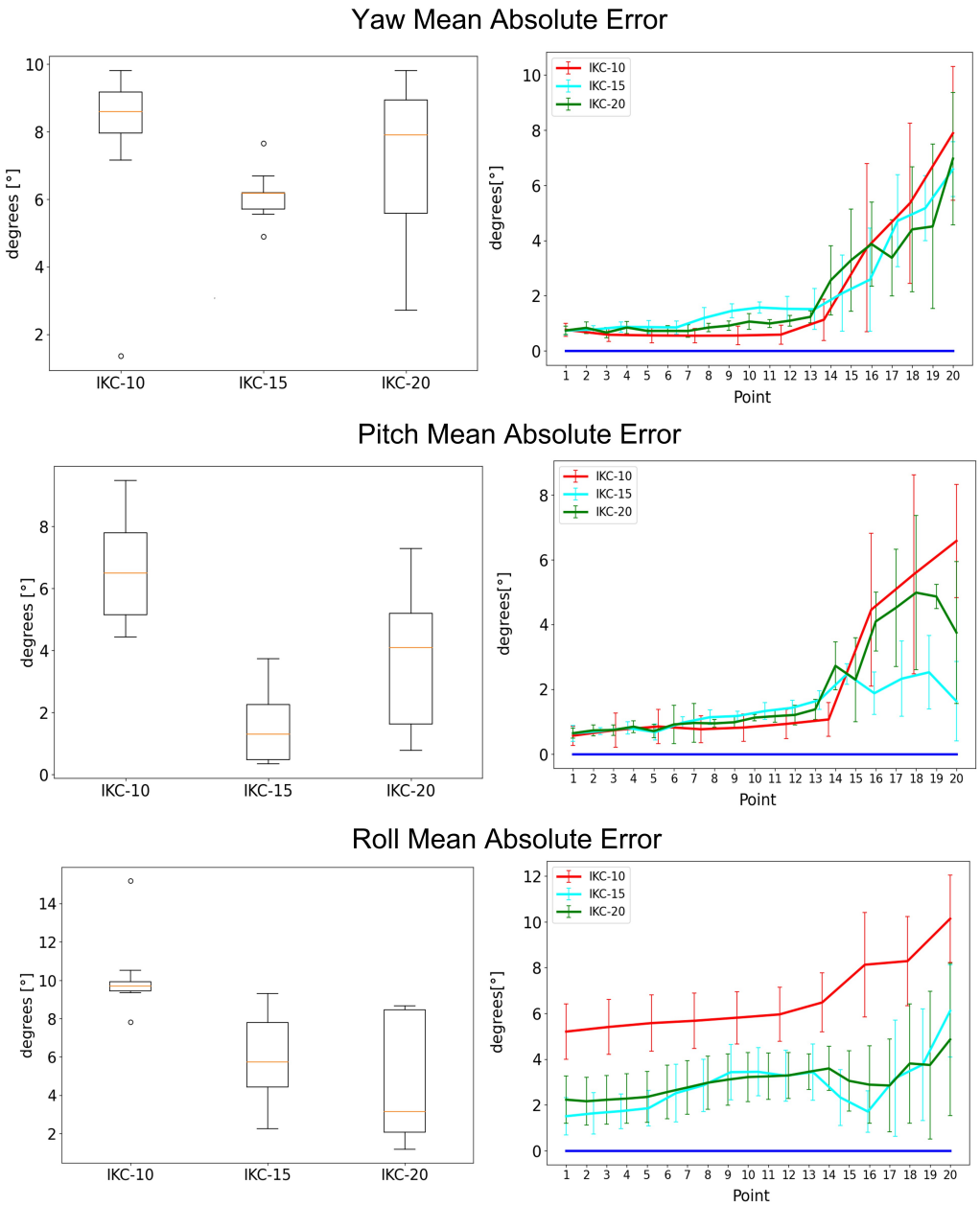

Figure 5.11: *IKC-10, IKC-15, IKC-20 Orientation Mean Absolute Error. On the left: yaw, pitch and roll angles along path's points. On the right: yaw, pitch and roll target points MAE.*

Lastly, the normality assessment on the target point error distribution is conducted resulting in yaw, pitch and roll angles MAE being normally distributed, thus the errors can be described by *mean-value* and *standard deviation*. For the three experiments, the results are summarized in Table 5.1.

Target *mean value* ± *standard deviation* [°]			
	Yaw	**Pitch**	**Roll**
IKC-10	7.88 ± 2.42	6.67 ± 1.74	10.13 ± 1.91
IKC-15	6.13 ± 0.72	3.63 ± 1.22	5.80 ± 2.33
IKC-20	6.96 ± 2.39	3.74 ± 2.14	4.98 ± 3.17

Table 5.1: *Results from model-free IKC-10, IKC-15 and IKC-20 experiments. In particular, mean value and standard deviation error on target point is displayed for yaw, pitch, roll angles.*

6 | Discussion

Throughout this chapter, it will be provided a comprehensive overview of the results obtained in the experiments, by examining the outcomes reported in chapter 5.

6.1. Controller Accuracy

The efficacy and accuracy of the controller is analysed for each experiment, both for the path tracking task and the target point errors. In particular, a comparison between the accuracy of two approaches is evaluated:

- model-free controller (**IKC-5**) over a model-based one (**PID-5**);
- model-free characterization with respect to path's number of points (**IKC** over **5**, **10**, **15** and **20** path points).

It is important to note that, the four paths' repetitions do not change significantly the results for any of the experiments, as reported in Appendix A. This can be a consequence that the whole system lies in static environment conditions, without external disturbances. Thus, the tested controllers can be defined as deterministic, i.e. giving the same results when given the same inputs, under stable external conditions. Furthermore, no significant differences emerged from the analysis of the error in the Cartesian axes **x**, **y** and **z**, so only points ED is analysed and discussed.

6.1.1. Model-free versus Model-based Results Analysis

As reported in Sections 5.1.1 5.1.2 and 5.1.3, the different combinations of catheter's bending do not influences significantly the two controller accuracy for path tracking task, both in position ED and orientation MAE. For the model-free approach, it can be due to a good training dataset that covers the whole workspace of the catheter, with all possible bending combinations being mapped in the training phase. The model-based approach instead, uses an analytical model fitted to the physical properties of the tendon-driven MC system, making the ML and AP motions coherent for all bendings, with a PID

compensating for the errors on both planes in the same way.

Since the resulting data are non-normally distributed, path tracking accuracy can be characterized by the *median* and *quartiles* values. Here, it is demonstrated that the errors appear higher for the model-based approach rather then the model-free ones (Table of Figure 6.1).

In addition, this trend can be also observed in the last target point error. Indeed, the accuracy is not the same for all path's points, with the error increasing when approaching the target. This behaviour is due to the increased DoFs to control, since the first points to reach are mainly characterized by catheter's insertion with small bending, while last points do require also a control for higher bendings values in both ML and AP planes. It is reported that the errors on the target points are normally distributed in both model-free and model-based experiments, so they can be described by the *mean-value* and *standard deviation*, shown in Figure 6.1.

Euclidean Distance [mm]

Path Tracking		
	Model-free	Model-based
median	0.86	7.09
quartile 25%	0.82	6.99
quartile 75%	3.95	7.54

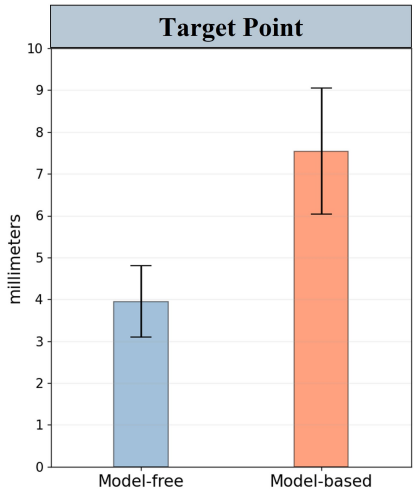

Figure 6.1: *Comparison between model-free and model-based Euclidean Distance for position path tracking (left) and target point (right).*

It is evident that, position errors are higher in the model-based approach rather than the model-free one, both for path tracking and target point analysis. In the experiments, model-based approach issues emerge: internal non-linearities as catheter hysteresis, tendons' backlash effect and inside torsions between Delivery and Guide Catheters, plus external factors as friction and gravity are not accounted in the MC modelling. Even in a closed-loop condition, the errors are not sufficiently compensated and corrected, since

PID control is a linear controller and its parameters have been manually tuned, thus they are likely to be suboptimal.

On the other hand, the model-free approach comprehends intrinsically those non-linearities, since the data used for the network training comes from the real catheter set-up. In addition, thanks to the sensor feedbacks and the learned non-linear mapping of the workspace, it is able to compute the appropriate outputs compensating the non-linear uncertainties.

However, non-negligible errors are still present, thus some investigations are performed. One source of error is due to sensors' accuracy (affecting both model-free and model-based approaches). Indeed, inside the volume generated by the FG, the RMSPE is 0.7 mm and 1.4 mm with a confidence interval of 95%. This is a large value, especially for the model-free network which highly relies on data.

Moreover, a physical fault has been observed in the real set-up. Many times, the control signals coming from the IKC Node sent to Arduino Node, are not correctly actuated, in particular when a change in the direction of the motor occurs (Figure 6.2).

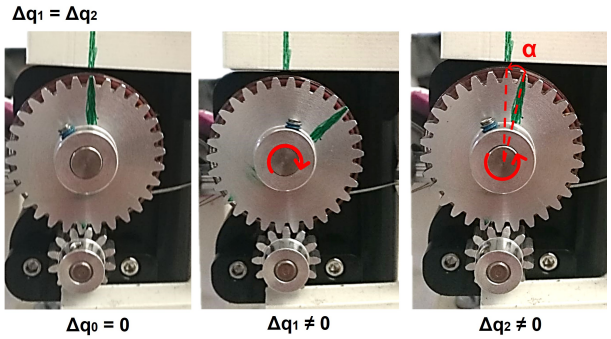

Figure 6.2: *Motor actuation error recorded on real set-up (ML motor example). From left to right: motor's state at initial position (Δq_0); a clockwise rotation (Δq_1); a counter-clockwise rotation ($\Delta q_2 = \Delta q_1$). A residual angle α can be observed that is approximately 12°, which corresponds to 2 mm tendon displacement error.*

Since the motors do not have integrated encoders, the actuators' state message, sent from Arduino Node to the IKC Node, is not based on a real value read from the motors, rather it is a variable updated at each iteration independently. Thus, even if the actuation is not executed, the updated motors state is delivered and used from the controller network to compute next motion.

Concerning the orientation, even though in [35] only position control has been taken into account, a comparison between angles MAE is performed to evaluate if the proposed controller improves the accuracy in terms of clip orientation requirements (Figure 6.3).

Mean Absolute Error [°]

		Path Tracking	
		Model-free	Model-based
Yaw	median	1.18	9.75
	quartile 25%	0.95	7.74
	quartile 75%	7.73	14.58
Pitch	median	1.14	7.45
	quartile 25%	0.94	7.40
	quartile 75%	5.31	9.82
Roll	median	6.17	3.52
	quartile 25%	5.98	3.22
	quartile 75%	8.42	7.25

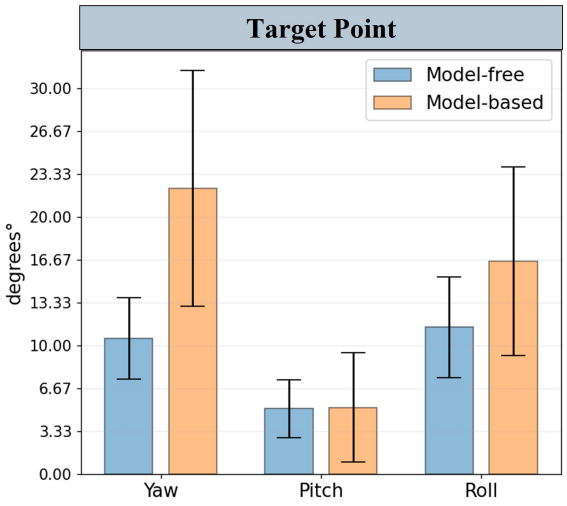

Figure 6.3: *Comparison between model-free and model-based Mean Absolute Error for orientation path tracking (left) and target point (right).*

The noticeable improvements makes the proposed controller also effective for orientation control, with a more complete controller due to its ability to regulate both position and orientation states of the MC robotic system, so higher end-effector controllability.

6.1.2. Path Points Results Analysis

Once having established the performances of the proposed model-free controller with respect to the state-of-the-art model-based one [35], it is convenient to assess its functionality in different conditions, characterizing the controller with respect to path's number of points to track. In Figure 6.4 the results from Sections 5.1.1 and 5.1.3 are summarized:

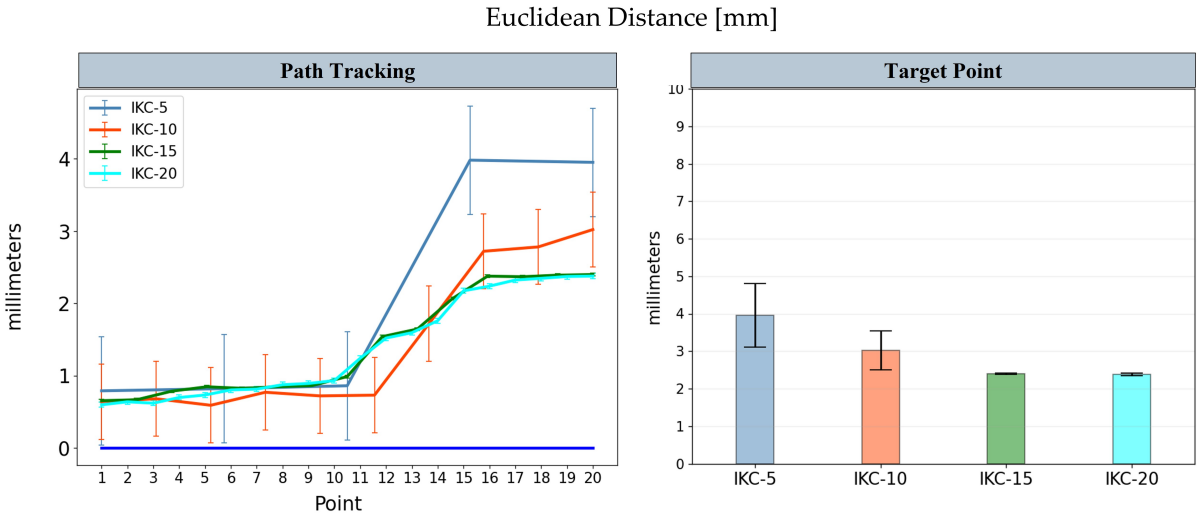

Figure 6.4: *Comparison between 5-points over 10-points, 15-points and 20-points position Euclidean Distance in path tracking (left) and target point (right).*

An additional investigation is executed to verify if the gartered data on target point are significantly different for the four experiments. In particular, the z-test is used for determining if two sample means are statistically different from each other. The z-test is a parametric test that assumes that the sample data is normally distributed and the population variance is known. The z-test works by calculating the z-score, which represents the number of standard deviations that a sample mean is from the population mean. The formula for calculating the z-score is expressed in Equation 6.1

$$z = \frac{\bar{x} - \mu}{\frac{\sigma}{\sqrt{n}}} \tag{6.1}$$

where:

$\bar{x}$ is the sample mean;

μ is the population mean;

σ is the population standard deviation;

n is the sample size.

If the absolute value of the calculated z-score is greater than the *critical-value* at a chosen significance level, then it is possible to reject the null hypothesis that the sample means are equal and conclude that there is a statistically significant difference between them.

With this tests, it is demonstrated that all the experiments sample means differ one from another, except for the experiments *IKC-15* and *IKC-20*, that instead results equal.

From this comparison, it can be demonstrated that the increased number of points improves the controller performances in position accuracy until a certain range of path points. The reason why this happens is investigated. In general, when moving a polymeric material that shows non-linear and hysteresis properties, slow and smaller steps can help to reduce the effects of the non-linearities. This is because slow and gradual movements can allow the material to adjust and respond more smoothly to the applied forces, which can reduce the amount of energy that is lost as heat due to the internal friction in the material [32]. Additionally, by moving the material in small steps, the hysteresis effect can be minimized by keeping the material within a range of deformation where its response is relatively predic and consistent, while whit higher or forces, the material exceeds this range exhibiting more unpredictable behaviour, which can result in greater hysteresis effects [6].

Concerning the orientation, the resulting MAE for the four experiments is shown in Figure 6.5. By executing the z-test on the orientation data, as previously described, it results that there is no significant differences between the mean orientation samples, thus it can be concluded that the increase in number of points do not improve orientation accuracy. It can be observed that the lowest error is on the pitch angle, which is related to the AP plane bending angle. On the other hand, roll angle MAE is the highest, but this angle is the one associated to the rotation of the clip around its axis, which is not controlled in this work.

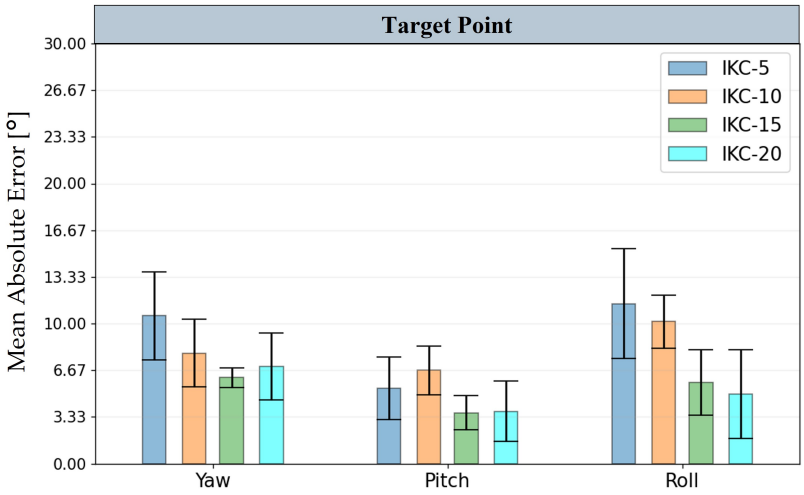

Figure 6.5: *comparison between 5-points over 10-points, 15-points and 20-points orientation Mean Absolute Error on target point.*

In general, yaw and pitch angle, which determine the perpendicularity of the clip with respect to the mitral valve plane, show errors below 10°, which is considered an acceptable range for the MC procedure.

7 | Conclusions and Future Developments

This final chapter will contain the conclusions about this thesis, overviewing the developed MC robotic system, highlighting its strengths and limitations that could possibly be overcome in future works.

MC Robotic System Overview

This thesis aimed at developing an autonomous control of a robotic surgical device for percutaneous minimally invasive SIC, in collaboration with European partners working together in the ARTERY project. This project aims at overcoming the limits of the manual commercially available MitraClip™ system, which is the current Gold Standard of percutaneous approach for mitral valve repair, by employing an innovative robot-assisted platform with autonomous control that cooperates with the surgeon for the success of this life-saving procedure. With this system, patients will benefit from a safer procedure, and interventionist will experience reduced mental workload and damaging radiations coming from imaging devices.

In previous work, a robotic actuation-platform for the MC system, coupled with a PID position control was developed. However, some limitations in the mechanical design and control algorithm are present.

Hence, this thesis presented two primary goals:

- re-design of the previous MC robotic system to include clinical requirements that were missing in its first prototype;
- implement a novel control algorithm that improves the performances in terms of position and orientation accuracy.

For the latter, a model-free closed-loop controller based on FNN was exploited. The reasons underlying this choice was to overcome limitations that a model-based approach

holds, mainly due to the multiple approximations needed to model non-linear systems as the MC. In addition, a PID controller, although being efficient in many applications, needs to be tuned, which is an extremely difficult challenge, thus making the controller more likely to be suboptimal. The developed IKC, based on neural networks, is able to learn a mapping between end-effector pose and system actuation throughout real data, which intrinsically comprehends all the non-linear internal and external factors, as hysteresis, tendon's backlash and friction. Thanks to the real-time feedbacks of the EM sensors, it is able to produce the needed actuation to reach a desired target within it workspace with good accuracy. Indeed, some experiments were carried out to evaluate its performances in path tracking task. The results discussed in Chapter 6, reported that this novel control improved the accuracy with respect to its previous implementation, reaching a position accuracy of 3 mm, and around 8° for orientation, which was not controlled by the PID.

Limitations

It's important to acknowledge that this work is subject to some limitations. For a mechanical point of view, the Device Handle, still misses a motorized actuation of the clip. Apart for the insertion, it still cannot rotate around its axis and move its arms and grippers. Thus, the application of the clip stays completely manual and is left in the surgeon's expert hands. Additionally, this system is built to work in the intra-cardiac part of the intervention, leaving out the intra-vascular Catheters insertion that would need a further linear actuator carrying the whole MC system.

From a point of view of the electrical components, only one Arduino Uno is used, which acts on the motors sequentially, not allowing a smooth contemporaneous motion of the motors. Moreover, some incorrect actuations were observed, as reported in Section 6.1.1. Due to Arduino's limited memory and reduced dimension, it is likely to become unusable if more actuators have to be introduced.

The sensorization part have also some drawbacks. In particular, EM sensors are highly susceptible to interference from electromagnetic sources, experiencing some degree of drift in calibration over time, particularly if they are exposed to uncontrolled environmental factors such as temperature fluctuations or mechanical stress, which can cause measurement errors.

For what concerns control, model-free controllers based on neural networks are highly dependent con data, thus they can be susceptible to noise and disturbances in the data. As an example electromagnetic interferences when using EM sensors can lead to poor performance. Susceptibility to noise and disturbances: neural network controllers can be

sensitive to noise and disturbances in the system, which can lead to poor performance. This can be a significant issue if the system is placed in uncontrolled and unpredictable environment. In addition, model-free neural network controllers are typically trained on a specific task and do not generalize well to other tasks or different environments.

Future Developments

The limitations described above may constitute the object of future works. Still some mechanical components are needed to make this system a fully autonomous robotic platform, from the intravascular insertion to the intra-cardiac intervention. In re-designing the actuation system, it could be useful to introduce a more performant micro-controller as the Raspberry Pi, which is a powerful processor with more memory than the Arduino, and have also has built-in support for networking, which makes it ideal for projects that require communication with other devices. Then, by introducing encoders it is possible to always have knowledge about motors state, thus improving a low-level control. A different sensorization strategy can be adopted, for example by using Fiber Bragg Grating optical sensors that are less sensitive to environmental disturbances, thus being more suitable for data-driven control approaches. Lastly, different controller architectures can be exploited as Recursive or Radial Basis Function networks, which are suited for adaptive control able to compensate the effect of highly non-linear, time-dependent systems.

In conclusion, the control of autonomous robotic platforms for minimally-invasive percutaneous procedures is an important challenge because of many non-linear intrinsic and extrinsic factors present is such systems. Model-free controllers have an high potential in overcoming limitations of traditional control approaches, especially in non-linear system as continuum robots, thus making them suitable for catheterization procedures.

Bibliography

[1] A. Ali, A. Sakes, et al. Catheter steering in interventional cardiology: Mechanical analysis and novel solution. *Proc. Inst. Mech. Eng. H*, 233(12):1207–1218, Dec. 2019. ISSN 2041-3033. doi: 10.1177/0954411919877709.

[2] A. A. Alqumsan, S. Khoo, et al. Robust control of continuum robots using Cosserat rod theory. *Mech. Mach. Theory*, 131:48–61, Jan. 2019. ISSN 0094-114X. doi: 10.1016/j.mechmachtheory.2018.09.011.

[3] Y. Ansari, M. Manti, et al. Multiobjective Optimization for Stiffness and Position Control in a Soft Robot Arm Module. *IEEE Rob. Autom. Lett.*, 3(1):108–115, July 2017. ISSN 2377-3766. doi: 10.1109/LRA.2017.2734247.

[4] M. Barbanti, S. Buccheri, et al. Transcatheter or surgical treatment of severe aortic stenosis and coronary artery disease: A comparative analysis from the Italian OBSERVANT study. *Int. J. Cardiol.*, 270:102–106, 2018. ISSN 1874-1754. doi: 10.1016/j.ijcard.2018.06.011.

[5] I. Belluschi, N. Buzzatti, et al. The Alfieri's edge-to-edge technique for mitral valve repair: from a historical milestone of cardiac surgery to the origin of the transcatheter era. *Mini-invasive Surgery*, 4:58, Sept. 2020. doi: 10.20517/2574-1225.2020.48.

[6] V. Beloshenko, Y. Beygelzimer, et al. Strain hysteresis of polymers. *Dokl. Phys. Chem.*, 409:207–209, Jan. 2006. doi: 10.1134/S0012501606070086.

[7] S. Bhagat, H. Banerjee, et al. Deep Reinforcement Learning for Soft, Flexible Robots: Brief Review with Impending Challenges. *Robotics*, 2019.

[8] S. Bhattacherjee, S. Chattopadhayay, et al. Kinematics and Teleoperation of Tendon Driven Continuum Robot. *Procedia Comput. Sci.*, 133:879–886, Jan. 2018. ISSN 1877-0509. doi: 10.1016/j.procs.2018.07.106.

[9] M. Birger and A. S. K. et al. Spending on cardiovascular disease and cardiovascular risk factors in the united states: 1996 to 2016. *Circulation*, 144:271–282, 7 2021. ISSN 15244539. doi: 10.1161/CIRCULATIONAHA.120.053216.

[10] S. Boutaleb, E. Racine, et al. Performance and suitability assessment of a real-time 3D electromagnetic needle tracking system for interstitial brachytherapy. *Journal of Contemporary Brachytherapy*, 4:280–289, Sept. 2015. doi: 10.5114/jcb.2015.54062.

[11] J. M. Boyce, G. Potter-Bynoe, et al. Hospital reimbursement patterns among patients with surgical wound infections following open heart surgery. *Infect. Control Hosp. Epidemiol.*, 11(2):89–95, Feb. 1990. ISSN 0899-823X. doi: 10.2307/30144267.

[12] J. Burgner-Kahrs, D. C. Rucker, et al. Continuum Robots for Medical Applications: A Survey. *IEEE Trans. Rob.*, 31(6):1261–1280, Nov. 2015. doi: 10.1109/TRO.2015.2489500.

[13] D. B. Camarillo, C. F. Milne, et al. Mechanics Modeling of Tendon-Driven Continuum Manipulators. *IEEE Trans. Rob.*, 24(6):1262–1273, Dec. 2008. ISSN 1552-3098. doi: 10.1109/TRO.2008.2002311.

[14] D. B. Camarillo, C. R. Carlson, et al. Task-Space Control of Continuum Manipulators with Coupled Tendon Drive. In *Experimental Robotics*, pages 271–280. Springer, Berlin, Germany, 2009. doi: 10.1007/978-3-642-00196-3_32.

[15] A. Centurelli. Closed-loop Control of Soft-Robots using Reinforcement Learning, Apr. 2021.

[16] K. Chin, T. Hellebrekers, et al. Machine Learning for Soft Robotic Sensing and Control. *Adv. Intell. Syst.*, 2(6):1900171, June 2020. ISSN 2640-4567. doi: 10.1002/aisy.201900171.

[17] P. Cominos and N. Munro. PID controllers: recent tuning methods and design to specification. *IEE Proceedings - Control Theory and Applications*, 149(1):46–53, Jan. 2002. ISSN 1359-7035. doi: 10.1049/ip-cta:20020103.

[18] O. De Backer, I. Wong, et al. Transcatheter mitral valve repair: an overview of current and future devices. *Open Heart*, 8(1):e001564, Apr. 2021. ISSN 2053-3624. doi: 10.1136/openhrt-2020-001564.

[19] M. De Bonis, E. Lapenna, et al. Edge-to-edge alfieri technique for mitral valve repair. *Curr. Opin. Cardiol.*, 28(2):152, Mar. 2013. ISSN 0268-4705. doi: 10.1097/HCO.0b013e32835b9256.

[20] C. Della Santina, C. Duriez, et al. Model Based Control of Soft Robots: A Survey of the State of the Art and Open Challenges. *arXiv*, Oct. 2021. doi: 10.48550/arXiv.2110.01358.

[21] J. Eschmann. Reward Function Design in Reinforcement Learning. In *Reinforcement Learning Algorithms: Analysis and Applications*, pages 25–33. Springer, Cham, Switzerland, Jan. 2021. doi: 10.1007/978-3-030-41188-6_3.

[22] F. N. N. et al. Imaging in structural heart disease: The evolution of a new subspecialty. *JACC: Case Reports*, Oct. 2019.

[23] G. A. R. et al. Global burden of cardiovascular diseases and risk factors, 1990–2019. *Journal of the American College of Cardiology*, 76:2982–3021, 12 2020. ISSN 07351097. doi: 10.1016/j.jacc.2020.11.010.

[24] M. Faggioni and R. Mehran. Preventing Contrast-induced Renal Failure: A Guide. *Interv. Cardiol.*, 11(2):98–104, Oct. 2016. ISSN 1756-1477. doi: 10.15420/icr.2016:10:2.

[25] T. George Thuruthel, Y. Ansari, et al. Control Strategies for Soft Robotic Manipulators: A Survey. *Soft Rob.*, 5, Jan. 2018. doi: 10.1089/soro.2017.0007.

[26] C. M. Gibson, S. Korjian, et al. Safety and Tolerability of CSL112, a Reconstituted, Infusible, Plasma-Derived Apolipoprotein A-I, After Acute Myocardial Infarction. *Circulation*, Dec. 2016.

[27] M. Giorelli, F. Renda, et al. A feed-forward neural network learning the inverse kinetics of a soft cable-driven manipulator moving in three-dimensional space. In *2013 IEEE/RSJ International Conference on Intelligent Robots and Systems*, pages 5033–5039. IEEE, Nov. 2013. doi: 10.1109/IROS.2013.6697084.

[28] M. Grube, J. C. Wieck, et al. Comparison of Modern Control Methods for Soft Robots. *Sensors*, 22(23):9464, Dec. 2022. ISSN 1424-8220. doi: 10.3390/s22239464.

[29] A. Harky et al. The Future of Open Heart Surgery in the Era of Robotic and Minimal Surgical Interventions. *Heart, Lung and Circulation*. doi: 10.1016/j.hlc.2019.05.170.

[30] P. Hyatt, C. C. Johnson, et al. Model Reference Predictive Adaptive Control for Large-Scale Soft Robots. *Front. Rob. AI*, 7, Oct. 2020. ISSN 2296-9144. doi: 10.3389/frobt.2020.558027.

[31] A. D. Jara Ram et al. Complications of Robotic Surgery. *Surg. Clin. North Am.*, 100(2):461–468, Apr. 2020. ISSN 1558-3171. doi: 10.1016/j.suc.2019.12.008.

[32] K. K. Kar and A. K. Bhowmick. Analysis of high strain hysteresis loss of nonlinear rubbery polymer. *Polym. Eng. Sci.*, 38(1):38–48, Jan. 1998. ISSN 0032-3888. doi: 10.1002/pen.10163.

[33] M. Li, R. Kang, et al. Design and control of a tendon-driven continuum robot. *Trans. Inst. Meas. Control*, 40(11):3263–3272, Mar. 2017. ISSN 0142-3312. doi: 10.1177/0142331216685607.

[34] M. J. Mack, M. B. Leon, et al. Transcatheter Aortic-Valve Replacement with a Balloon-Expandable Valve in Low-Risk Patients. *N. Engl. J. Med.*, 380(18):1695–1705, Mar. 2019. ISSN 1533-4406. doi: 10.1056/NEJMoa1814052.

[35] M. Magro. Robotic actuation and autonomous control of a tendon-driven catheter for structural intervention cardiology, Apr. 2022.

[36] T. Mahl, A. Mayer, et al. A variable curvature modeling approach for kinematic control of continuum manipulators. *2013 American Control Conference*, 2013.

[37] A. D. Marchese, K. Komorowski, et al. Design and control of a soft and continuously deformable 2D robotic manipulation system. In *2014 IEEE International Conference on Robotics and Automation (ICRA)*, pages 2189–2196. IEEE, May 2014. ISBN 978-1-4799-3685-4. doi: 10.1109/ICRA.2014.6907161.

[38] A. Martin-Barrio, S. Terrile, et al. Modelling the Soft Robot Kyma Based on Real-Time Finite Element Method. *Comput. Graphics Forum*, 39(6):289–302, Sept. 2020. ISSN 0167-7055. doi: 10.1111/cgf.14026.

[39] P. Modi, A. Hassan, et al. Minimally invasive mitral valve surgery: a systematic review and meta-analysis. *Eur. J. Cardiothorac. Surg.*, 34(5):943–952, Nov. 2008. ISSN 1010-7940. doi: 10.1016/j.ejcts.2008.07.057.

[40] M. D. Molly Szerlip, M. D. Konstantinos S. Spargias, et al. 2-Year Outcomes for Transcatheter Repair in Patients With Mitral Regurgitation From the CLASP Study. *Cardiovascular Interventions*, July 2021. doi: 10.1016/j.jcin.2021.04.001.

[41] T.-D. Nguyen and J. Burgner-Kahrs. A tendon-driven continuum robot with extensible sections. *2015 IEEE/RSJ International Conference on Intelligent Robots and Systems (IROS)*, pages 2130–2135, Sept. 2015. doi: 10.1109/IROS.2015.7353661.

[42] D. Paparella and K. e. a. Fattouch. Current trends in mitral valve surgery: A multicenter national comparison between full-sternotomy and minimally-invasive approach. *Int. J. Cardiol.*, 306:147–151, May 2020. ISSN 0167-5273. doi: 10.1016/j.ijcard.2019.11.137.

[43] V. Parcha, N. Patel, et al. Mortality Due to Mitral Regurgitation Among Adults in the United States: 1999-2018. *Mayo Clin. Proc.*, 95(12):2633–2643, Dec. 2020. ISSN 0025-6196. doi: 10.1016/j.mayocp.2020.08.039.

[44] B. Pawlowski. Modeling, simulation, and control of soft robots. *Colorado State University. Libraries*, Dec. 2018.

[45] R. S. Penning, J. Jung, et al. An evaluation of closed-loop control options for continuum manipulators. *2012 IEEE International Conference on Robotics and Automation*, 2012.

[46] a. o. Pique, Francesco. A learning-based approach for adaptive closed-loop control of a soft robotic arm. Dec. 2020.

[47] A. Püschel, C. Schafmayer, et al. Robot-assisted techniques in vascular and endovascular surgery. *Langenbecks Arch. Surg.*, 407(5):1789–1795, Aug. 2022. ISSN 1435-2451. doi: 10.1007/s00423-022-02465-0.

[48] P. Rao, Q. Peyron, et al. How to Model Tendon-Driven Continuum Robots and Benchmark Modelling Performance. *Front. Rob. AI*, 7, Feb. 2021. ISSN 2296-9144. doi: 10.3389/frobt.2020.630245.

[49] R. F. Reinhart, Z. Shareef, et al. Hybrid Analytical and Data-Driven Modeling for Feed-Forward Robot Control †. *Sensors*, 17(2):311, Feb. 2017. ISSN 1424-8220. doi: 10.3390/s17020311.

[50] F. Renda, C. Armanini, et al. Geometrically-Exact Inverse Kinematic Control of Soft Manipulators With General Threadlike Actuators' Routing. *IEEE Rob. Autom. Lett.*, 7(3):7311–7318, June 2022. ISSN 2377-3766. doi: 10.1109/LRA.2022.3183248.

[51] G. Robinson and J. Davies. Continuum robots - a state of the art. *Proceedings 1999 IEEE International Conference on Robotics and Automation (Cat. No.99CH36288C)*, 1999.

[52] M. Rolf and J. J. Steil. Efficient Exploratory Learning of Inverse Kinematics on a Bionic Elephant Trunk. *IEEE Trans. Neural Networks Learn. Syst.*, 25(6):1147–1160, Nov. 2013. ISSN 2162-2388. doi: 10.1109/TNNLS.2013.2287890.

[53] D. Rus and M. T. Tolley. Design, fabrication and control of soft robots. *Nature*, 521 (7553):467–475, May 2015. ISSN 1476-4687. doi: 10.1038/nature14543.

[54] A. H. Sepehripour, G. Garas, et al. Robotics in cardiac surgery. *Ann. R. Coll. Surg. Engl.*, 100(Suppl 7):22, Sept. 2018. doi: 10.1308/rcsann.supp2.22.

[55] P. L. Steinberg, P. A. Merguerian, et al. A da Vinci Robot System Can Make Sense for a Mature Laparoscopic Prostatectomy Program. *JSLS*, 12(1):9, Jan. 2008.

[56] B. Sun, W. Li, et al. Recent Progress in Modeling and Control of Bio-Inspired

Fish Robots. *Journal of Marine Science and Engineering*, 10:773, June 2022. doi: 10.3390/jmse10060773.

[57] T. Takuma. Design of Tendon-Driven Mechanism Using Geometrical Condition. *Actuators*, 9(3):48, June 2020. ISSN 2076-0825. doi: 10.3390/act9030048.

[58] T. G. Thuruthel, E. Falotico, et al. Learning Closed Loop Kinematic Controllers for Continuum Manipulators in Unstructured Environments. *Soft Rob.*, 4(3):285–296, Sept. 2017. ISSN 2169-5180. doi: 10.1089/soro.2016.0051.

[59] T. G. Thuruthel, E. Falotico, et al. Stable Open Loop Control of Soft Robotic Manipulators. *IEEE Rob. Autom. Lett.*, 3(2):1292–1298, 2018. ISSN 2377-3766. doi: 10.1109/LRA.2018.2797241.

[60] V. P. e. a. Timmis Adam. European Society of Cardiology: cardiovascular disease statistics 2021. *Eur. Heart J.*, 43(8):716–799, Feb. 2022. ISSN 0195-668X. doi: 10.1093/eurheartj/ehab892.

[61] J. Wang and A. Chortos. Control Strategies for Soft Robot Systems. *Adv. Intell. Syst.*, 4(5):2100165, May 2022. ISSN 2640-4567. doi: 10.1002/aisy.202100165.

[62] J. G. Webb, M. Hensey, et al. 1-Year Outcomes for Transcatheter Repair in Patients With Mitral Regurgitation From the CLASP Study. *JACC Cardiovasc. Interv.*, 13 (20):2344–2357, Oct. 2020. ISSN 1876-7605. doi: 10.1016/j.jcin.2020.06.019.

[63] Q. Wu, Y. Gu, et al. Position Control of Cable-Driven Robotic Soft Arm Based on Deep Reinforcement Learning. *Information*, 11(6):310, June 2020. ISSN 2078-2489. doi: 10.3390/info11060310.

[64] F. Yanagawa, M. Perez, et al. Critical Outcomes in Nonrobotic vs Robotic-Assisted Cardiac Surgery. *JAMA Surg.*, 150(8):771–777, Aug. 2015. ISSN 2168-6262. doi: 10.1001/jamasurg.2015.1098.

[65] L. Young. Robotic Percutaneous Coronary Intervention: The Good, the Bad, and What is to Come, Sept. 2021.

[66] T. Zheng, Q. Han, et al. Task Space Tracking of Soft Manipulators: Inner-Outer Loop Control Based on Cosserat-Rod Models. *arXiv*, Oct. 2022. doi: 10.48550/arXiv.2210.00976.

A | Appendix A

As described in Section 4.2, each path is repeated four times, thus the distribution of the position and orientation data measured for each trial is analysed through qualitative and quantitative tests as boxplots and the two-sample Kolmogorov-Smirnov (KS).

The KS test is a non-parametric statistical test that can be used for comparing the underlying distribution of a sample $F(x)$ with a known distribution (e.g. normal, uniform, etc.) or with another sample $G(x)$, returning the corresponding test's *statistic* and *p-value*. The null hypothesis of this tests is that the two distributions are identical, $F(x) = G(x)$ for all x; the alternative is that they are not identical. The *statistic* is the maximum absolute difference between the empirical distribution functions of the samples. If the *p-value* is greater than 0.05, the null hypotheses cannot be rejected, so there is not enough evidence to support the claim that the two distributions $F(x)$ and $G(x)$ are different.

If all the repetitions of a path result belonging to the same distribution, this data can be averaged and considered as a single one. Otherwise, each repetition must be studied and discussed individually.

Another important consideration about the measured data, is to understand if they belong to a normal distribution. For the normality tests, visual inspection through QQ-plots and quantitative tests as KS and Shapiro-Wilk (SW) tests are performed. Differently from KS, the SW test is a parametric statistical test used for determining whether a given sample of data comes from a normally distributed population. Thus, the null hypothesis is that the sample comes from a normally distributed population, and the alternative hypothesis is that it does not. The test calculates a test *statistic*, a measure of how closely the sample data follows a normal distribution, and the *p-value*. As for the KS test, if the *p-value* is greater than 0.05, the null hypotheses cannot be rejected, so there is not enough evidence to support the claim that the data is not normally distributed.

If the samples are normally distributed, mean and standard deviation can be considered as test's metrics, otherwise median and quartiles become the most appropriate ones.

These evaluations are performed for all experiments (**IKC-5**, **PID-5** ,**IKC-10**, **IKC-15**, **IKC-20**), and for both position and orientation metrics (ED, MAE).

A.1. Euclidean Distance

For the data collected in the experiments, the distribution analysis of the four repetitions is performed on position ED and orientation MAE.

In all 9 paths, both qualitative and quantitative analysis prove that the repetitions belong to the same distribution. For this reason, each repetition can be grouped and averaged with the others belonging to the same path. One example is shown in Figure A.1.

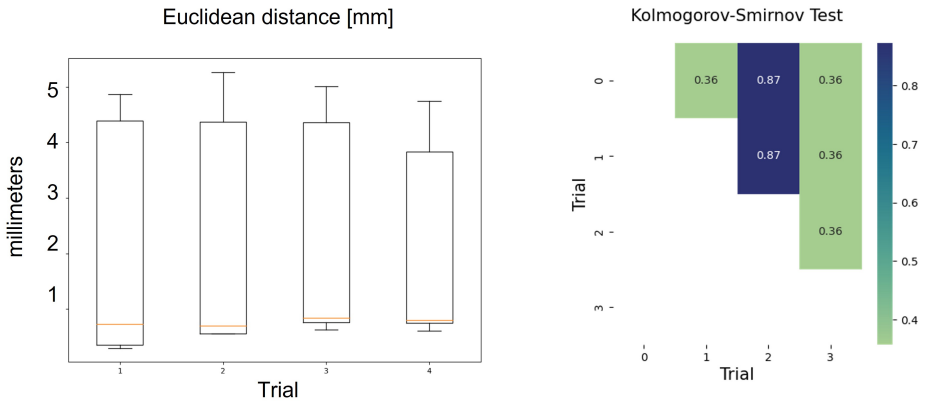

Figure A.1: *Repetitions Distribution. On the left: quantitative analysis of path repetition through box-plots. On the right: quantitative analysis of samples distribution KS test expressed through a map showing the p-value of coupled trials' samples.*

Concerning the normality assessment, the qualitative QQ-plot evaluation is shown in Figure A.2.

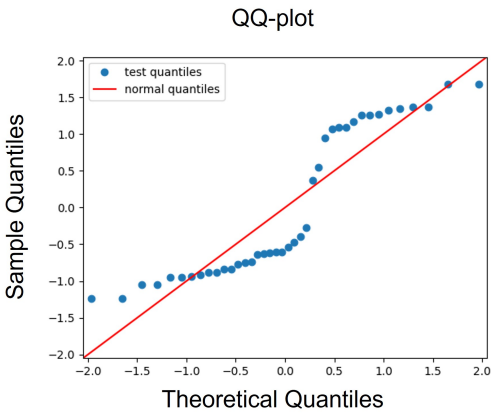

Figure A.2: *QQ-plot qualitative analysis for normality assessment of the experimental data.*

This visual inspection, together with the quantitative results of the KS and SW tests ($p\text{-}value < 0.05$), supports the rejection of the null hypotheses of normality.

A.2. Orientation Mean Absolute Error

The same ideas of distribution assessment is followed in the analysis of yaw pitch and roll MAE. Also in this case, qualitative and quantitative analysis prove that the repetitions belong to the same distribution for all paths, each repetition can be grouped and averaged with the others belonging to the same path and that this distribution is non-normal for all angles (Figure A.3).

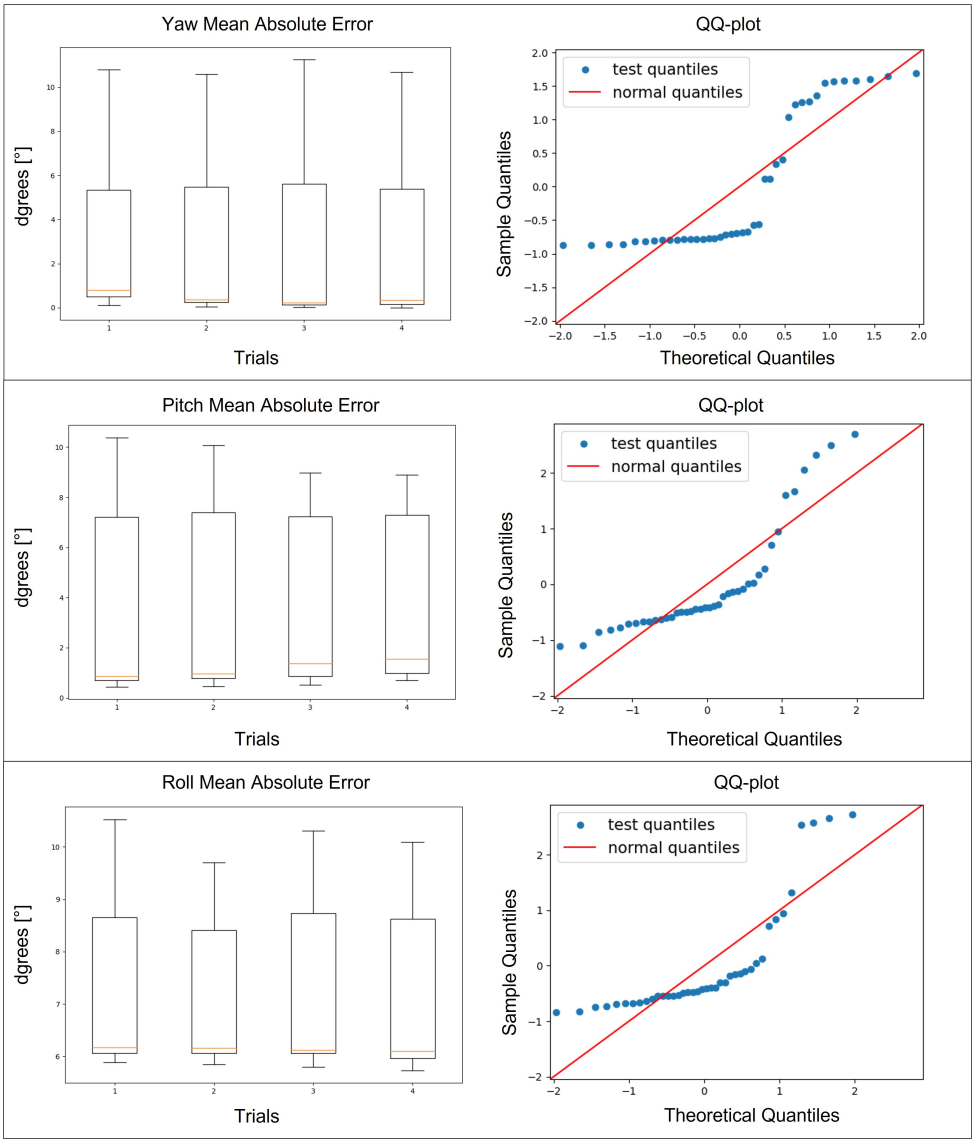

Figure A.3: *Yaw, Pitch and Roll MAE box-plots and QQ-plots for quantitative and qualitative analysis of samples distribution and normality.*

List of Figures

List of Tables

List of Abbreviations

CVD Cardiovascular Disease

SHD Structural Heart Disease

MR Mitral Regurgitation

MVP Mitral Valve Prolapse

SIC Structural Intervention Cardiology

RT3DTEE Real-Time 3D Transesophageal Echocardiography

TMVr Transcatheter Mitral Valve repair

ML Medial-Lateral

AP Anterior-Posterior

MC MitraClip™

ABS Acrylonitrile Butadiene Styrene

DoF Degrees of Freedom

PRB Pseudo Rigid Body

CC Constant Curvature

PCC Piecewise Constant Curvature

VR Variable Curvature

CR Cosserat Rod

PID Proportional Integral Derivative

NN Neural Network

MLP Multi-Layer Perceptron

FNN Feedforward Neural Network

RL Reinforcement Learning

DRL Deep Reinforcement Learning

IKC Inverse Kinematic Controller

EM Electromagnetic

SCU System Control Unit

SIU Sensor Interface Unit

FG Field Generator

RMSPE Root Mean Squared Position Error

ROS Robot Operating System

ED Euclidean Distance

MAE Mean Absolute Error

RF Reference Frame

IKC-5 Inverse Kinematic Controller 5-points Experiment

PID-5 Model-based PID controller 5-points Experiment

IKC-5 Inverse Kinematic Controller 10-points Experiment

KS Kolmogorov-Smirnov

SW Shapiro-Wilk